Diploma Thesis

Sensitivity Analysis as a Tool in Hygrothermal Component Analysis

submitted in satisfaction of the requirements for the degree
Diplom-Ingenieur
of the TU Wien, Faculty of Civil and Environmental Engineering

---

Diplomarbeit

Sensitivitätsanalyse als Werkzeug in der hygrothermischen Bauteilanalyse

ausgeführt zum Zwecke der Erlangung des akademischen Grads
Diplom-Ingenieur
eingereicht an der TU Wien, Fakultät für Bau- und Umweltingenieurwesen

Florian Schnabel, BSc

Matr.Nr.: 11807470

Betreuung: Prof. Dipl.-Ing. Dr.techn. **Thomas Bednar**
Dipl.-Ing. **Andreas Sarkany**, BSc
Institute of Material Technology, Building Physics, and Building Ecology - E207
Research Unit Building Physics
Technische Universität Wien
Karlsplatz 13/E207-02, 1040 Wien, Österreich

Wien, im Oktober 2024 _____

Kurzfassung

Hygrothermisch Bauteilsimulation sind Werkzeuge, die es erlauben, Vorhersagen über das Verhalten und die Dauerhaftigkeit von Konstruktionen zu treffen. Derartige Simulationen bauen auf Eingangparameter, welchen jedoch eine Unsicherheit zugrunde liegt. Diese Unsicherheit in den Eingangsparametern zieht eine Unsicherheit in den Prognosen nach sich. Daher kann eine deterministische Herangehensweise möglicherweise unzureichend sein, um zuverlässige Vorhersagen zu treffen. Als Alternative bietet es sich an, eine stochastische Herangehensweise zu verfolgen. Eine derartige Herangehensweise erlaubt die Bewertung einer Konstruktion basierend auf einer Versagenwahrscheinlichkeit, anstelle der binären Aussage Versagen oder kein Versagen. Zusätzlich ermöglicht sie den Zugang zu weiteren stochastischen Analysemethoden, wie zum Beispiel Sensitivitätsanalysen. Dabei handelt es sich um Methoden, die im Allgemeinen eine Abschätzung des Zusammenhangs zwischen Eingangparametern und resultierenden Zustandsgrößen liefern. Derartige Zusammenhänge können Informationen über eine Reihe von Modelleigenschaften, wie Modellverhalten, Relevanz der Eingangsparameter, Modellstabilität oder mögliches Optimierungspotenzial, liefern. Mit dem Potenzial der stochastischen Analysemethoden kommt jedoch auch ein Bedarf für mehr Eingangsparameter, mehr Rechenaufwand und die Entwicklung von Methoden zur Einschätzung der Zuverlässigkeit der Aussagen. Diese Arbeit beschäftigt sich mit der Anwendbarkeit von Sensitivitätsanalyse im Zusammenhang mit hygrothermischer Bauteilsimulation. Zwei verschiede Sensitivitätsanalysemethoden werden implementiert und ihre Anwendbarkeit in drei Beispielen untersucht. Eine integrierte Methode zur Abschätzung der Zuverlässigkeit der Aussagen wird vorgeschlagen. Die Ergebnisse zeigen, dass die untersuchten Sensitivitätsanalysemethoden in der Lage sind, das Modellverhalten und Schlüsselparameter zu identifizieren. Deutliche Unterschiede im Konvergenzverhalten der beiden Methoden werden festgestellt. Konfidenzintervalle zeigen sich als hilfreiches Kriterium für die Konvergenz von Sensitivitäten. Ihr alleiniger Einsatz zur Sicherstellung der Zuverlässigkeit der Sensitivitäten ist jedoch nicht ausreichend, da sie im Falle einer Methode nicht dazu in der Lage sind, das Versagen der Methode aufzuzeigen. Abschließend wird gezeigt, dass die Anwendung von Sensitivitätsanalyse Unterstützung in der Modelloptimierung liefern kann.

Abstract

Hygrothermal simulations are tools to predict the reliability and behaviour of a building component. These simulations are based on input parameters, which are subject to significant uncertainty. The uncertainty in the input parameters results in a significant uncertainty in the model output. A deterministic approach may therefore not give a reliable prediction. As an alternative, a probabilistic approach can be followed. Such an approach allows for an evaluation of the component based on a probability of failure instead of a binary failed or not failed. Additionally, this allows applying stochastic analysis methods, such as Sensitivity Analysis (SA). In the most general sense, SA is a tool to estimate input output relations of models. These relations can provide information on a range of properties, for example model behaviour, relevance of input parameters, model stability, or optimization potential. However, the potential of stochastic analysis introduces the need for additional input parameters, a higher computational effort and the development of methods to estimate its reliability. This work revolves around the applicability of SA in hygrothermal simulations on component level. Two different methods of SA are explored, and their application to hygrothermal analysis is tested on three cases. An in the process integrated method to estimate the reliability of resulting sensitivities is proposed. The results show that the investigated SA methods are capable of identifying general model behaviour and identify key parameters. Significant differences in the convergence behaviour of the methods have been observed. Confidence intervals provide a useful indication for the convergence. However, confidence intervals alone are not sufficient in indicating the reliability of the estimated sensitivity, as they fail to identify failure for one of the methods for low sample sizes. Finally, it is demonstrated that SA can provide reliable guidance in model optimisation.

Contents

Acronyms

SA Sensitivity Analysis

FAST Fast Fourier Sampling Test

eFAST extended Fast Fourier Sampling Test

LHC Latin Hypercube Sampling

Symbols

h	...	enthalpy density J/m^3
$\mathbf{q}$	...	density of heat flow rate in W/m^2
s_q	...	heat production rate in W/m^3
w	...	moisture content kg/m^3
$\mathbf{g}$	...	density of moisture flow rate in kg/(m^{3}s)
s_g	...	moisture production rate in kg/(m^{3}s)
ρ_a	...	density of air in kg/m^3
V_a	...	pore volume of air in m^3/m^3
$\mathbf{r}$	...	density of air flow rate in kg/(m^{3}s)
s_r	...	air production rate in kg/(m^{3}s)
q_k	...	density of conductive heat flow rate in W/m^2
q_c	...	density of convective heat flow rate in W/m^2
$c_{p,a}$	...	specific heat capacity of dry air in J K/kg
λ	...	thermal conductivity in K m W
T	...	temperature in K
q_{sol}	...	density of solar heat flow rate in W/m^2
α	...	absorptivity in -
I_{sol}	...	solar radiation in W/m^2
q_{sky}	...	density of atmospheric heat flow rate in W/m^2
ε^*	...	effektive emissivity in -
σ	...	Stefan-Boltzmann constant
$\mathbf{n}$	...	normal vector in -
$\mathbf{g_v}$	...	density of vapourous moisture flow rate in kg/(m^{3}s)
$\mathbf{g_l}$	...	density of liquid moisture flow rate in kg/(m^{3}s)
$\mathbf{g_{v,diff}}$	...	density of diffusive vapourous moisture flow rate in kg/(m^{3}s)
$\boldsymbol{\delta}_v$	...	vapour permeability in kg/(m^{2}sPa)
$\boldsymbol{K}$	...	liquid conductivity in s
$\boldsymbol{C}$	...	permeance in kg Pa m/s
$\boldsymbol{k}$	...	permeability in m^2
μ	...	dynamic viscosity of air in N s/m^2
$S_i(\bullet)$	...	Sensitivity Indices of the ith variable
$D(\bullet)$	...	variance of $\bullet$
$D(\bullet)_i$	...	partial variance of $\bullet$ as a result of the i'th variable

Chapter 1

Introduction

Hygrothermal simulations on component level aim to predict the temperature and moisture state in building components, as a result of exposure to indoor and outdoor climate and their material properties. The reliability of this prediction is both dependent on the quality of the hygrothermal model itself and the quality of the simulation parameters (Pang et al., 2020). In the case of hygrothermal simulations, many of these parameters are subject to significant uncertainties (Zhao et al., 2015). For some parameters these uncertainties are quantified through measurements, for example the uncertainty in the heat conductivity of a material. In other cases the information on the parameter itself is sparse, and an assumption has to be made by the analyst. Examples are the wide range for absorptivity of the exterior surface, the sorption isotherms of materials, or the airtightness of the envelope. (Bednar, 2000; Nusser, 2012; Wissenschaftlich-Technische Arbeitsgemeinschaft für Bauwerkserhaltung und Denkmalpflege, 2016). A deterministic simulation based on uncertain parameters may not give reliable predictions on the components' behaviour. This led to the development of various probabilistic approaches to hygrothermal simulations Zhao et al. (2021).

Following a probabilistic approach provides significant advantages. Upfront it provides access to the probability of failure as a criterion for the reliability of a construction (Hopfe and Hensen, 2011). Various failure models can be used to formulate failure criteria, in this work moisture accumulation and mould growth are used (Ojanen et al., 2011). This is by no means sufficient for the full assessment of a component. Additional criteria and possible models can be found in Austrian standards ("ÖNORMB 8110-2 - Wärmeschutz im Hochbau - Teil 2," 2020). The probabilistic evaluation of these failure criteria then allows the quantification of the risk associated with the component. In addition to risk assessment, this approach also allows the application of stochastic analysis methods, which can be used to gain additional information on the model behaviour. Of particular interest for this work are methods combined under the term SA. In most general sense, these give an estimation for the relation between the model input and output.

The application of SA on hygrothermal simulations has been investigated numerous times. In the context of building simulations, a comparison of different SA was done in the IEA Annex 55, where different SA methods have been applied to the cold attics model. Twelve different methods were investigated in their ability to analyse a model with 14 uncertain input parameters. (Hagentoft et al., 2015; Hagentoft, 2011). Pang et al. (2020) reviewed the application of SA in building performance modelling in 96 case-studies, resulting in a condensed list of

recommendations on how to perform SA. On the building component level it was shown that SA can be used to identify relevant model parameters (Panico et al., 2023). Zhao et al. (2011) showed its capabilities to derive additional information on model behaviour on basis of an Wall Assembly. The former uses the Morris screening method, the latter uses Pearson Correlation Coefficients, to gain information on complex input output relations. The combination of those approaches, referred to as a hybrid SA approach, can potentially allow for a reduction of computational effort of probabilistic simulations, while maintaining reliable information on the input output relation of critical parameters (Pang et al., 2020).

In this work we want to investigate the applicability of SA as a general tool in hygrothermal analysis on component level. Concerning the difficulties revolving around SA that surface repeatedly in literature, we want to address the following points:

Computational Effort As the probabilistic approach is inherently tied to increased computational effort, it is crucial to reduce the sample size as much as possible. Different methods are followed to achieve this. In the context of SA one possibility is the use of screening methods, applied to a smaller sample, to identify impactful parameters and neglect insignificant ones. Another approach is to replace the model itself by a metamodel to reduce the number of simulations to run. An investigation of this can be found in (Hagentoft et al., 2015). This approach has gained popularity in combination with variance based SA (Pang et al., 2020). The needed sample size can as well be reduced through the use of efficient sampling methods, in building simulation Latin Hypercube Sampling (LHC) sampling is commonly used. Overall, a combination of these approaches is advisable.

Uncertainty of Input In Addition to the computational effort, a probabilistic method raises the question of the probability distribution of the uncertain variables. The uncertainty of the model input directly affects the uncertainty of the model output. As stated in Zhao et al. (2015), due to the lack of knowledge on the variables itself, often the judgment of the analyst is needed to decide on the scale of the uncertainty. Pang et al. (2020) states this lack of knowledge on the uncertainty levels of the variables reduces the reliability of the SA.

Indication of Reliability Another question arising when applying SA, is the reliability of the resulting sensitivities. For one, the sensitivities are only estimations and therefore subject to uncertainties themselves. The sample size and quality needed, for the sensitivities to stabilize, is both dependent on the SA method and the analysed case. Even though minimum sample sizes are proposed for some SA method, these are not necessarily sufficient in all cases (Pang et al., 2020; Saltelli et al., 1999). Additionally, as different SA methods are not equivalent, they do not necessarily stabilize to identical sensitivities. In the context of building science this has been shown in numerous cases (Hagentoft et al., 2015; Pang et al., 2020).

In this work we want to investigate the applicability of SA. This is done on basis of the following research questions.

- Is SA as a tool in hygrothermal analysis able to identify the relation between local effects in the state variables and the parameters leading to these effects?
- Is SA as a tool in hygrothermal analysis robust enough to provide reliable results for low sample sizes?
- Are confidence intervals, estimated through bootstrapping, able to estimate the reliability of the sensitivities resulting from a SA?
- Are results of a SA able to directly guide analyst in how to improve failing building components?

Before these questions can be investigated the fundamentals of hygrothermal models, the field of SA and fitting models for this task are explored in Chapter 2. Then a simulation framework, which extends the used simulation software to allow for a probabilistic approach and SA, is developed in Chapter 2. With the software architecture established, the research questions are then investigated on basis of a case study consisting of three examples.

Chapter 2

Methodology

This section deals with the mathematical and physical foundation of the methods employed in this work. At first the mathematical properties of the underlying simulations are explored (Sec. 2.1) and with the resulting possibilities and restrictions in mind, the field of Sensitivity Analysis is then outlined (Sec. 2.2), and fitting methods are chosen. These methods and the ideas behind them are then further elaborated. The chapter is concluded with a Section dedicated to the role of confidence intervals and an approach to estimate them (Sec. 2.3).

2.1 Hygrothermal Simulations

In the field of building science, Hygrothermal Simulations are used to describe heat, air, and moisture transport. In this work the simulation domain is restricted to the building component level. The used approach to describe these phenomena is through a combination of various partially coupled sub-problems. The mathematical properties of this system of differential equations, are relevant to apply fitting analysis methods. Therefore, this section deals with the mathematical models used in hygrothermal simulations, with the aim to provide a basis, for making assumptions about the model behaviour.

The discussed physical phenomena can be described by models of varying complexity (Bednar, 2000; Hagentoft, 2001; Hens, 2017). The list of models mentioned in this work is restricted to models implemented in the used simulation software. It has to be noted, that the discussed models are by no means exhaustive.

The formulas and methods on the physical phenomena in this section are heavily based on (Bednar, 2000), where the basis for HAM4D_VIE, from this point on referred to as Ham4D, was developed. Ham4D is hygrothermal simulation software, which uses the Finite Volume Method to solve the in Sec. 2.1.1 described partial differential equations. From then on Ham4D was continuously extended or adapted for various use cases (Hinterseer, 2024; Sarkany, 2019; Sarkany and Bednar, 2021; Wegerer and Bednar, 2017). Not all of its capabilities are documented or published, therefore other publications, with similar approaches on the topic, are referenced, when describing the fundamental processes.

2.1.1 System of Differential Equations

A common approach (Bednar, 2000; Hagentoft, 2001; Hens, 2017) when describing the hygrothermal problem in a building component, is to use a system of coupled differential equations. The foundations of which are based on conservational laws for certain physical quantities. The conservation of the enthalpy density $h\,(\mathrm{J/m^3})$ links the density of the heat flow rate $\mathbf{q}\,(\mathrm{W/m^2})$ and the of the heat source $s_q\,(\mathrm{W/m^3})$ to the time evolution of the enthalpy.

$$\frac{\partial h(w)}{\partial t} = -\nabla \cdot \mathbf{q}(T, w) + s_q \tag{2.1}$$

Moisture conservation links the density of the moisture flow rate $\mathbf{g}(\mathrm{kg/(m^2\,s)})$ and the moisture source $s_g\,(\mathrm{kg/(m^3 s)})$ to the time evolution of the moisture density $w\,(\mathrm{kg/m^3})$

$$\frac{\partial w(T)}{\partial t} = -\nabla \cdot \mathbf{g}(w, T) + s_g\,. \tag{2.2}$$

The conservation of air mass density $m_a = \rho_a\, V_a\,(\mathrm{kg/m^3})$ links the density of air flow rate $r\,(\mathrm{kg/(m^2\,s)})$ to the evolution of air mass. For the typical use cases the air transfer is much more reactive than the heat and moisture transfer. For these use cases air can be considered incompressible (Hens, 2017) and therefore the change of the air mass can be approximated to be zero.

$$\frac{\partial(\rho_a\, V_a)}{\partial t} = -\nabla \cdot \mathbf{r}(T) + s_r \approx 0\,. \tag{2.3}$$

The coupling of these differential equations is rooted in the heat and mass flow rates and is either introduced by the driving forces or the material parameters.

2.1.2 Heat Transfer

The heat flow rate in a porous medium can be decompositioned into the densities of conductive $\mathbf{q}_k\,(\mathrm{W/m^2})$ and convective $\mathbf{q}_c\,(\mathrm{W/m^2})$ heat flow rate inside the medium

$$\mathbf{q} = \mathbf{q}_k + \mathbf{q}_c\,, \tag{2.4}$$

and to densities of radiative $\mathbf{q}_r\,(\mathrm{W/m^2})$ and convective $\mathbf{q}_c\,(\mathrm{W/m^2})$ heat flow rate for surfaces boundering fluid or gaseous domains as

$$\mathbf{q} = \mathbf{q}_r + \mathbf{q}_c\,. \tag{2.5}$$

The density of the conductive heat flow rate can be described by Fourier's Law

$$\mathbf{q}_k = -\boldsymbol{\lambda}(T, w) \cdot \nabla T\,, \tag{2.6}$$

with the gradient of the temperature as the driving force and the thermal conductivity $\lambda\,(\mathrm{W/mK})$. The convective heat transfer accounts for all the heat transferred by transporting a

liquid or gas through the medium. In general this includes both water and air. In the case of this work, both the heat transported by vapour, and the heat transported through liquid water is neglected. The density of the convective heat flow rate can then be written, independently of the moisture concentration, with the specific heat capacity of dry air $c_{p,a}$ (J/kgK), as:

$$\mathbf{q}_c = \mathbf{r}\, c_{p,a}\, T \tag{2.7}$$

It is common practice to split the radiative heat transport into low and high frequency heat transport. High frequency radiation representing gains through solar radiation and low frequency radiation representing gains and losses due to atmospheric radiation. For the usual temperatures of building components ($\approx 280\,\mathrm{K}$), the emission of high frequency radiation is neglectable. The density of the heat flow rate due to solar gains can be written as

$$\mathbf{q}_{sol} = \boldsymbol{\alpha} \cdot \mathbf{I}_{sol}\,, \tag{2.8}$$

with the absorptivity $\boldsymbol{\alpha}\,(-)$ for high frequencies and the solar radiation $I_{sol}\,(\mathrm{W/m^2})$. The density of the heat flow rate due to low frequency radiation can be described as

$$\mathbf{q}_{sky} = \varepsilon^*\, \sigma\, (T_s^4 - T_r^4)\, \mathbf{n} \tag{2.9}$$

with the effective emissivity $\varepsilon^*\,(-)$ for low frequencies, the *Stefan-Boltzmann constant* $\sigma = 5.67 \cdot 10^{-8}\,(\mathrm{W/m^2K^4})$ and $\mathbf{n}$ the normal vector of the surface. Due to $|T_s - T_r| \ll T_s, T_r$ linearization around $T = 280\,\mathrm{K}$ is justified (Bednar and Riccabona, 2013). With the further assumption of similar emissivities $\varepsilon_s \approx \varepsilon_r \longrightarrow \varepsilon^* \approx \varepsilon_s$, $\mathbf{q}_{sky}$ simplifies to

$$\mathbf{q}_{sky} \approx \varepsilon_s \cdot 5 \cdot (T_s - T_r)\, \mathbf{n}\,. \tag{2.10}$$

2.1.3 Moisture Transfer

Similar to the heat transfer phenomena, it is possible to define the density of moisture flow rate as a superposition of the densities of vapourous $\mathbf{g}_v\,(\mathrm{kg/m^2s})$ and liquid $\mathbf{g}_l\,(\mathrm{kg/m^2s})$ moisture flow rates.

$$\mathbf{g} = \mathbf{g}_v + \mathbf{g}_l \tag{2.11}$$

Two phenomena of vaporous moisture transport are considered. Diffusive transport, driven by the gradient of the partial vapour pressure $p_{vap}\,(\mathrm{Pa})$, described by Fick's Law

$$\mathbf{g}_{\mathbf{v,diff}} = -\boldsymbol{\delta}_v \cdot \nabla p_{vap}\,, \tag{2.12}$$

with the water vapour permeability $\boldsymbol{\delta}_v\,(\mathrm{kg/m^2sPa})$. And convective transport through air mass transport

$$\mathbf{g_{v,conv}} = \frac{0.622\ \mathbf{r_a}}{p_a - p_{vap}} \approx 6.21 \cdot 10^{-6}\, p_{vap}\, \mathbf{r_a}\,. \tag{2.13}$$

This approximation is applicable for temperatures below 50 °C and pressure differences small compared to the atmospheric pressure (Hens, 2017). Liquid water transport as a result of interaction forces between the liquid and solid phases, can be homogenized to a suction pressure p_{suc} (Pa). The transport is then driven by the gradient of the suction pressure and can be defined as

$$\mathbf{g_l} = \mathbf{K}(w, T) \cdot \nabla p_{suc}\,, \tag{2.14}$$

with the liquid conductivity $\mathbf{K}$ (s). As elaborated in (Bednar, 2000) the suction pressure can then be related to the vapour pressure using the Kelvin equation.

2.1.4 Air Transfer

The air-flow in a porous medium can be described by the partial differential equation Eq. 2.3. As moisture and heat transfer are significantly slower processes than air transport, the description of air as an incompressible fluid is seen as sufficient. This allows the use of the steady state solution for the pressure field (Hens, 2017) and the density of the air flow rate can be expressed as

$$\mathbf{r}_a = -\mathbf{C} \cdot \nabla(P_{a,o} - \rho_a(T)\, \mathbf{g} \cdot \mathbf{z})\,. \tag{2.15}$$

The air pressure $P_{a,o}$ (Pa) accounts for forced convection and atmospheric pressure, and the temperature dependent pressure $(\rho_a(T)\, \mathbf{g} \cdot \mathbf{z})$ accounts for natural convection. An equation to calculate the permeance $\mathbf{C}$ (kg/(s Pa m)) can be derived from Darcy's law (Hagentoft, 2001) as

$$\mathbf{C} = \frac{\rho_a}{\mu}\, \mathbf{k}\,, \tag{2.16}$$

with the permeability of the medium $\mathbf{k}$ (m^2) and the dynamic viscosity of air μ (N s/m^2). For air flowing around the material in gaps, joints and cavities another model is needed. In this case a common approach is to model the flow as a hydraulic circuit (Hens, 2017). In Ham4D a simplified version of this is implemented, describing the air flow, considering all gaps and cavities of the building component, as

$$r_a = C\, \Delta P^b\,. \tag{2.17}$$

Values for the air flow coefficient C (m^3/(s Pa^b)) can for example be found in (Nusser, 2012).

2.2 Sensitivity Analysis

After having explored the physical foundations of the model, this section turns towards methods, which allow us to gain insight on the behaviour of the model, without explicit formulation of the

model itself. SA is a tool which can help to achieve this. (Saltelli et al., 2000, p. 4) proposes the following definition of SA :

> "Sensitivity Analysis studies the relationship between information flowing in and out of the model"

This additional information about the relation between the input and output of a model helps to answer the questions: Which input parameters have the most relevant contribution to the output and how can the input space be adapted to achieve a desirable output.

SA, in the context of this work, calls for an abstraction of the formulations explored in Sec. 2.1, which themselves are abstractions of the real world. The system of differential equations, the transport equations and the transport parameter models create a boundary value problem, which as a whole can be represented by an abstract model. The inputs of this model are the starting conditions, the boundary values and the material properties. The output of the model is the time evolution of field variables. Fig. 2.1 shows an illustration of such a model.

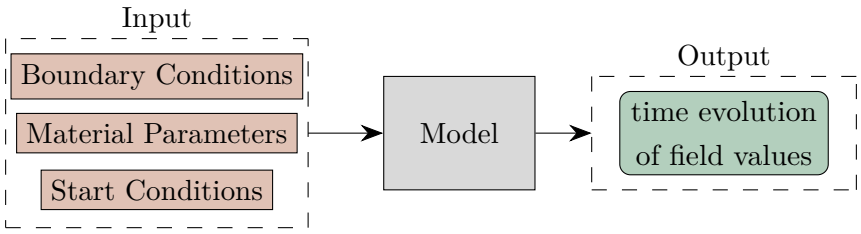

Fig. 2.1: Abstraction of the model

Even though no explicit formulation of the model itself is needed, there are characteristics which restrict what SA methods are applicable. As elaborated in (Camplolongo et al., 2000) the difficulty of the used analysis method increases with the model pathology. Prominent criteria are

- non-linearity,
- non-monotonicity,
- non-additivity.

Even if it is not always possible to define how the model behaves in respect to these criteria a priori, a better understanding of the model allows ruling out inapplicable SA methods. Therefore, before going forward in discussing different methods of SA, the formulations explored in Sec. 2.1 are examined in respect to the above-mentioned criteria.

2.2.1 Model Behaviour

Hygrothermal simulation do not always compute the whole range of transport phenomena listed in Sec. 2.1. For example, if there is no driving rain reaching the surface of a facade, it can be advisable to neglect the liquid water transport. In this section the behaviour of the very basis of the simulation in respect to linearity, monotonicity and additivity is analysed. As a starting

point heat transport through conduction is chosen. Specialization of Eq. 2.1 for $s_g = 0$, $q = q_c$, $w = 0$, $\lambda(T) = const.$, and Eq. 2.6 gives

$$\rho \, c_p \, \frac{\partial T}{\partial t} = \nabla \cdot (\boldsymbol{\lambda} \cdot \nabla T) \tag{2.18}$$

In Baehr (2008) various problem setups are discussed, for which analytical solutions for thermal conduction have been found. One of these setups is cooling and heating of simple bodies. We investigate one dimensional heat transport in a plate with a constant initial temperature $T(x, t = 0) = T_0$. The boundary conditions are constant in time $T(x = 0, t) = 0$ and $T(x = l, t) = 0$. The solution of the differential equation Eq. 2.18 for this setup can be found in (Baehr, 2008) as

$$T(x,t) = T_0 \left[\sum_{i=1}^{\infty} c_i \, \cos(\mu_i \, \frac{x}{l}) \, e^{-\mu_i^2 \, \frac{\lambda}{\rho \, c} \, \frac{t}{l^2}} \right] \tag{2.19}$$

In reference to the abstraction depicted in Fig. 2.1, we identify the heat conductivity λ as a model input and therefore investigate the behaviour of $T(x, t)$ at any $x > 0$ and $t > 0$ in λ. To test for monotony in λ, zeros of the first derivative of T in respect to λ are of interest. Assuming the sum $\left[\sum_{i=1}^{\infty} c_i \, \cos(\mu_i \, \frac{x}{l}) \, e^{-\mu_i^2 \, \frac{\lambda}{\rho \, c} \, \frac{t}{l^2}}\right]$ converges uniformly, allows for application of the differential operator to the summands, which yields

$$\frac{\partial T(\lambda)}{\partial \lambda} = -T_0 \left[\sum_{i=1}^{\infty} c_i \, \cos(\mu_i \, \frac{x}{l}) \, e^{-\mu_i^2 \, \frac{\lambda}{\rho \, c} \, \frac{t}{l^2}} \mu_i^2 \, \frac{t}{\rho \, c \, l^2} \right] \tag{2.20}$$

For $t > 0$, positive material parameters $\rho, c, l > 0$, non-zero start temperatures $T_0 \neq 0$, and consideration of $\mu_i^2 > 0$ only the term

$$\sum_{i=1}^{\infty} c_i \, \cos(\mu_i \, \frac{x}{l}) \, e^{-\mu_i^2 \, \frac{\lambda}{\rho \, c} \, \frac{t}{l^2}} \tag{2.21}$$

could allow for zeros. We further investigate the parts of the summands. As shown in (Baehr, 2008), the Fourier coefficients c_i and the eigenvalues μ_i show the following behaviour:

$$(i-1)\pi < \mu_i < \frac{(2i-1)\pi}{2} \qquad c_i = \frac{2 \, sin(\mu_i)}{\mu_i + sin(\mu_i) \, \cos(\mu_i)} \, . \tag{2.22}$$

For any $i \in \mathbb{N}$, μ_i is thus limited to being element of the first $0 < \mu_i < \pi/2$ and third quadrant $\pi < \mu_i < 3\,\pi/2$. The denominator in c_i can be thus be characterised as

$$\mu_i + sin(\mu_i) \, \cos(\mu_i) > 0 \quad \forall i \in \mathbb{N} \tag{2.23}$$

which implies

$$\begin{aligned} \cos(\mu_i \, \frac{x}{l}) > 0 \ \wedge \ c_i > 0 \quad \forall i \in \mathbb{N}_{odd} \, , \\ \cos(\mu_i \, \frac{x}{l}) < 0 \ \wedge \ c_i < 0 \quad \forall i \in \mathbb{N}_{even} \end{aligned} \tag{2.24}$$

and therefore

$$c_i \cos(\mu_i \frac{x}{l}) > 0 \quad \forall i \in \mathbb{N}\,. \tag{2.25}$$

Furthermore

$$e^{-\mu_i^2 \frac{\lambda}{\rho\, c} \frac{t}{l^2}} > 0\,, \tag{2.26}$$

from which it follows that all summands in Eq. 2.20 are positive. Therefore, $\frac{\partial T(\lambda)}{\partial \lambda}$ has no zeros for $\lambda > 0$. This implies that the sign of $\frac{\partial T(\lambda)}{\partial \lambda}$ does not change for $\lambda > 0$, thus $T(\lambda)$ is monotone in $\lambda > 0$.

But we do not want to restrict ourselves to constant boundary conditions. Therefore, we raise the complexity to allow for instationary (periodic) boundary conditions. Such a problem setup could for example be used to estimate the penetration depth of daily temperature changes in a building component. It is modelled, similarly as before, as a one dimensional problem, but now with only one periodic boundary condition $T(x = 0, t)$ at the surface. The analytical solution for the temperature field at any depth $x > 0$ and any time $t > 0$, for a heat transfer coefficient on the surface $\alpha \to \infty$ and the boundary condition

$$T(x = 0, t) = T_0(t) = T_m + \Delta T \cos(\omega\, t) = T_m + \Delta T \cos(2\pi \frac{t}{t_0})\,, \tag{2.27}$$

can be written according to (Baehr, 2008) as

$$T(x, t) = T_m + \Delta T\, e^{-\frac{\pi\, x \sqrt{\rho\, c}}{\sqrt{\pi\, \lambda\, t_0}}} \cos\left(2\pi \left(\frac{t}{t_0} - \frac{x\sqrt{\rho\, c}}{\sqrt{\pi\, \lambda\, t_0}}\right)\right)\,. \tag{2.28}$$

Following a similar approach to the first example, the derivative of the temperature in respect to λ is of interest. To increase readability we introduce $a(\lambda)$

$$a(\lambda) = \frac{\sqrt{\pi\, c\, \rho}\, \Delta T\, t_0\, x\, e^{-\frac{\pi\, x \sqrt{\rho\, c}}{\sqrt{\pi\, \lambda\, t_0}}}}{(t_0\, \lambda)^{3/2}}\,, \tag{2.29}$$

which for c, ρ, t_0, x, $\lambda > 0$ has no zeros. The derivative of the temperature in respect to λ can then be written as

$$\frac{\partial T(\lambda)}{\partial \lambda} = a(\lambda) \left[\cos\left(2\pi \left(\frac{t}{t_0} - \frac{x\sqrt{\rho\, c}}{2\sqrt{\pi\, \lambda\, T_0}}\right)\right) - 2 \sin\left(2\pi \left(\frac{t}{t_0} - \frac{x\sqrt{\rho\, c}}{2\sqrt{\pi\, \lambda\, T_0}}\right)\right)\right]\,. \tag{2.30}$$

As the sinus and cosinus term share the same argument, the term will equal zero for

$$\frac{t}{t_0} - \frac{x\sqrt{\rho\, c}}{2\sqrt{\pi\, \lambda\, T_0}} = \pi\, n + \tan^{-1}(1/2) \qquad \forall n \in \mathbb{N}\,. \tag{2.31}$$

For $0 < \lambda < \infty$ this allows for zeros in $\frac{\partial T(\lambda)}{\partial \lambda}$, $T(\lambda)$ is therefore non-monotone. Assuming $T(\lambda)$ is continuous in $\lambda > 0$, then the non-monotony implies that $T(\lambda)$ is non-linear, and non-additiv as well.

As one dimensional instationary heat conduction provides the basis for the investigated hygrothermal problems, it is to be expected, that more complex problems are non-linear, non-additiv, and non-monotone as well. With this established, a sufficient SA method needs to be found.

2.2.2 Types of Sensitivity Analysis Methods

As there are many different approaches to SA, a short overview on the main groups and some of their most prominent methods is given. (Camplolongo et al., 2000) lists the following categories:

- factor screening
- local Sensitivity Analysis
- global Sensitivity Analysis

Camplolongo et al. (2000) proposes factor screening for models with high numbers of uncertain parameters, which can be reduced before applying more computationally expensive methods. One way to achieve this, is through one-at-a-time experiments. In these experiments for each parameter two extreme values and a default value are identified. The numerical experiments are then carried out with one parameter in extreme position and all the other in default position. Subsequently, the sensitivity is represented by the difference in the output of the extreme and the output of the default configuration. One-at-a-time methods only allow for identification of main effects. To get information on interacting effects, more advanced screening methods (e.g. fractorial factorial design) are needed. Examples can be found in (Hagentoft et al., 2015) in building science specific context and (Camplolongo et al., 2000) for factor screening methods in a more general context.

Local SA describes the effects of the inputs on a local point through analytical methods. A prominent example is Differential Analysis. Camplolongo et al. (2000) describes the method in four steps. First the defaults and ranges for each input parameter are selected. Followed by the approximation of the output through a Taylor series. Variance propagation methods are then used to estimate the variance of the output and finally the impact of the individual parameters are estimated using the Taylor series approximations. It is often used in combination with a spatially homogeneous constant-parameter system. To allow for non-constant-parameter system, more advanced Differential Analysis methods (e.g. generalized sensitivity density) can be used.

Global SA describes the impact through a relation between input certainty and output certainty. Prominent fields in Global SA are Monte-Carlo-Based methods and Measures of Importance. Monte-Carlo-Based methods are done through evaluation of multiple experiments with randomly selected inputs. Examples for *correlation measures* and *two-sample tests* can be found in

(Hagentoft et al., 2015). The latter being further explored in Sec. 2.2.4. Measures of Importance are based on describing Sensitivity through

$$\frac{Var_{X_i}[E(Y|X_j = x_j)]}{Var(Y)}\,, \tag{2.32}$$

in which Var_{X_i} describes the variance over all possible values for X_j and $Var(Y)$ the total variance of the output. Two different methods to achieve this are through *Sobol' Sensitivity Indices* (Sobol, 2001) and Fast Fourier Sampling Test (FAST) developed in (Cukier et al., 1973). The latter being further explored in Sec. 2.2.3.

Considering the listed SA methods, with the insights about the model behaviour from Sec. 2.2.1 in mind, it is now possible to make a more profound decision on which SA method to use.

Screening methods allow for reduction of parameters, at the restriction of only providing quantitative results. In this work we assume, that relevant parameters have been identified a priori and a quantitative estimation of the direct and interactive effect of them is of interest. Therefore, screening methods are not sufficient for this use case.

As the FAST method allows for estimation of sensitivity in multiple orders and is applicable to non-monotone models with inhomogen parameter functions, it is chosen as the main method. As the segmentation based method is applicable to this model behaviour as well, and because it is computationally cheaper, it is selected as a comparison model.

2.2.3 Fourier Amplitude Sensitivity Test (FAST)

The FAST method has been developed in (Cukier et al., 1978; Cukier et al., 1973). The method used in this work will be an advanced version of FAST, named extended Fast Fourier Sampling Test (eFAST) developed in (Saltelli et al., 2010; Saltelli et al., 1999). The authors establish a model f in the form of

$$y = f(\mathbf{x})\,, \tag{2.33}$$

with the *k-dimensional* input vector $\mathbf{x}$ and the output y. The domain of the input is assumed to be a unit hypercube

$$K^n(\mathbf{x}|0 < x < 1, x_1, x_2, \ldots, x_n)\,, \tag{2.34}$$

and assuming $\mathbf{x}$ is a random vector with the density function $P(\mathbf{x}) = P(x_1, x_2, \ldots x_n)$, then the average of the outputs r'th moment $\langle y^{(r)} \rangle$ can be written as

$$\langle y^{(r)} \rangle = \int_{K^n} f(\mathbf{x}) P(\mathbf{x}) d\mathbf{x}\,. \tag{2.35}$$

$\langle y^{(r)} \rangle$ is of interest, as it provides information on the model's variance. According to (Cukier et al., 1978) a decomposition of the model's variance induced by the input parameters can be achieved through a multidimensional Fourier transformation. To avoid the computational

complexity of this multidimensional transformation, another approach is chosen. A search curve is introduced, which systematically explores the unit hypercube. The input parameters can be written as a function of a variable s and a set of frequencies ω_i as

$$x_i = G_i(\sin(\omega_i\, s))\,. \tag{2.36}$$

This introduces an oscillation in the input parameter x_i. Applying the model f this leads to an oscillation in the output y. This periodicity in the output now allows to perform a Fourier Analysis. The model can be written as a Fourier series

$$f(s) = \sum_{-\infty}^{\infty} A_j \cos(j\, s) + B_j \sin(j\, s)\,. \tag{2.37}$$

Furthermore, Cukier et al. (1973) shows that the Fourier coefficients can be connected to the variance induced by the parameters. Or in other words, if x_i shows a high impact on the output, the fourier transformed output will show a high amplitude at the frequencies $p\, w_i$. Assuming the search curve is space-filling, it is possible to evaluate the average of the outputs r'th moment in the s space as a one-dimensional integral along the search curve, as

$$\overline{y}^{(r)} = \lim_{t\to\infty} \frac{1}{2T} \int_{-T}^{T} f(\mathbf{x}(s))ds \tag{2.38}$$

In (Cukier et al., 1978) it is shown that for an incommensurate search curve the average in the s-space is equivalent to the average in the K-space.

$$\langle \overline{y}^{(r)} \rangle \equiv \overline{y}^{(r)} \tag{2.39}$$

Saltelli et al. (1999) states that due to the finite precision of computers, no set $\{\omega_i\}$ can be truly incommensurate. Therefore, the search curve will repeat itself at some point. Or, there is a positive rational number T so that $f(s) = f(s+T)$. For frequencies $\omega_i \in \mathbb{N}^+$ Cukier et al. (1973) shows that $T = 2\pi$. The formula for the Variance D as a function of the mean of the squared output, and the square of the mean output

$$D = \overline{(y^2)} - \overline{y}^2 \tag{2.40}$$

can be further specialised for Eq. 2.38 and Eq. 2.37, resulting in

$$\begin{aligned} D &= \frac{1}{2\pi}\int_{-\pi}^{\pi} f(\mathbf{x}(s))^2 ds - \left[\frac{1}{2\pi}\int_{-\pi}^{\pi} f(\mathbf{x}(s))ds\right]^2 \\ &= \frac{1}{2\pi}\int_{-\pi}^{\pi} \left[\sum_{j=-\infty}^{\infty} A_j \cos(j\, s) + B_j \sin(j\, s)\right]^2 ds - \left[\frac{1}{2\pi}\int_{-\pi}^{\pi} \sum_{j=-\infty}^{\infty} A_j \cos(j\, s) + B_j \sin(j\, s) ds\right]^2 . \end{aligned} \tag{2.41}$$

Using Parseval's therorem, and considering the symmetrie due to $f(s)$ being a real valued function ($A_j = A_{-j}$ and $B_j = B_{-j}$), Eq. 2.41 yields

$$D = \sum_{j \in \mathbb{Z}^0} C_j^2 = 2 \sum_{j=1}^{\infty} A_j^2 + B_j^2 = 2 \sum_{j=1}^{\infty} \Lambda_j \,, \tag{2.42}$$

with $\Lambda_j = A_j^2 + B_j^2$. Cukier et al. (1973) then state, that the variance of the output D_i induced by the input x_i, can be estimated by evaluating the spectrum of the frequency ω_i and its higher harmonics $p\,w_i$ with $p = 1, 2, ..., \infty$, as

$$D_i = 2 \sum_{p=1}^{\infty} A_{p\omega_i}^2 \,. \tag{2.43}$$

This partial variance D_i can now be used to estimate an index for the sensitivity as proposed in Eq. 2.32

$$S_{\omega_i} = \frac{D_i}{D} \,. \tag{2.44}$$

2.2.3.1 Search Curve Sampling

When using the FAST method, the sampling process is an essential part of the SA method. Different sampling methods are characterized through the chosen search curve Eq. 2.36. The aim is to create uniformly distributed samples in the unit hypercube K. In (Saltelli et al., 1999) different transformations are compared. This Section shall only give a short list of proposed transformations, and a visual representation of the resulting sampling distributions. (Cukier et al., 1973) proposed

$$x_i = \overline{x}_i \, e^{\overline{v}_i \, sin(\omega_i \, s)} \tag{2.45}$$

with the nominal value $\overline{x}_i$ and $\overline{v}_i$ a factor describing the endpoints of the estimated range. In (Koda et al., 1979) the authors proposed

$$x_i = \overline{x}_i \, (1 + \overline{v}_i \, sin(\omega_i \, s)) \,, \tag{2.46}$$

and in (Saltelli et al., 1999) both

$$x_i = \frac{1}{2} + \frac{1}{\pi} \arcsin(\sin(\omega_i \, s)) \,, \tag{2.47}$$

and an adaption by applying an additional phase shift

$$x_i = \frac{1}{2} + \frac{1}{\pi} \arcsin(\sin(\omega_i \, s) + \varphi_i) \,, \tag{2.48}$$

are proposed. Fig. 2.2 shows an illustration of how the samples are distributed in a two dimensional K-space $K(x_1, x_2)$ for each search curve. The evaluation is done for 250 samples and the frequencies $\omega = \{11, 21\}$. For Eq. 2.45 $\overline{x}_i = e^{-5}$ and $\overline{v}_i = 5$ are used. For Eq. 2.46 $\overline{x}_i = 1/2$ and $\overline{v}_i = 1$ are used. As well as a phase shift $\varphi = \{3.74, 3.98\}$.

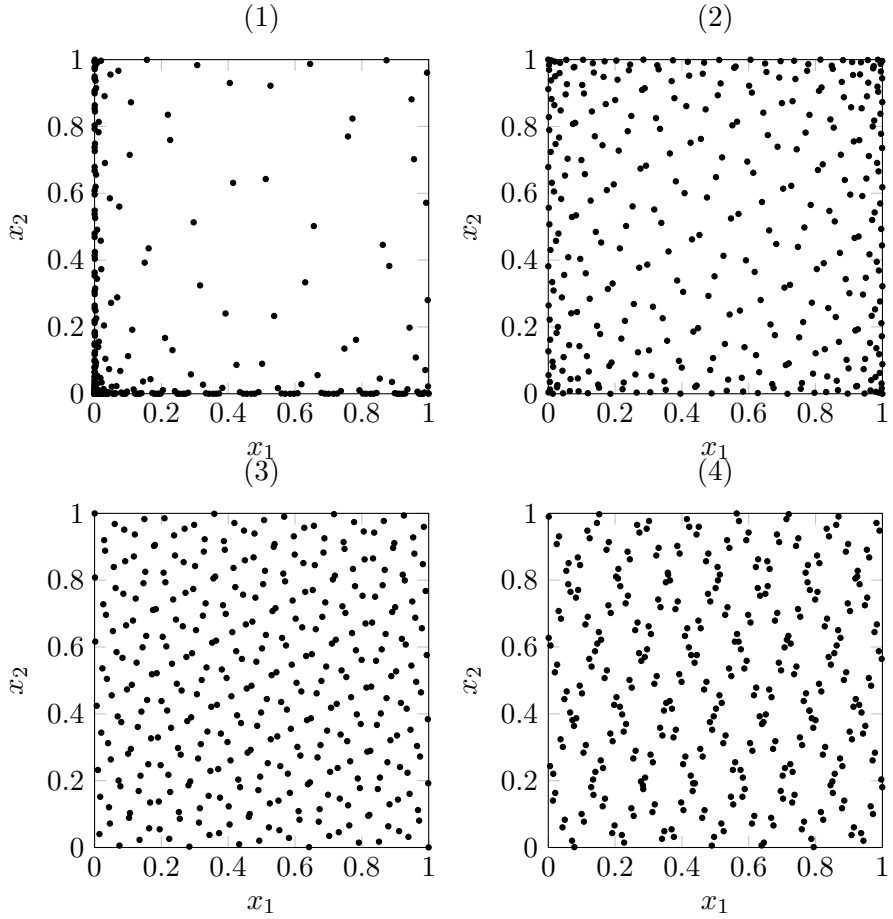

Fig. 2.2: Distribution of samples in the K-space using search curves according to equation 2.45 (1), equation 2.46 (2), equation 2.47 (3), and equation 2.48 (4)

The phase shift applied in Eq. 2.48 results in a loss of symmetry in $f(x)$ and therefore $x_i(s)$ has to be sampled for $s \in (-\pi, \pi)$ instead. The authors introduce *resampling* for using a unique phase shift for each variable φ_i and in the following compute the estimate for the Sensitivity Index for each variable from each curve. In Fig. 2.3 such a set is created, for three variables $\mathbf{x} = \{x_1, x_2, x_3\}$, $N = 500$, and $M = 4$. The interference factor M defines how many higher Harmonics are considered in Eq. 2.43, the infinite sum is truncated at $p = M$. The Sensitivity Index for each variable is then computed from its respective curve. In other words, the output y_i $\forall i = 1, 2, \ldots, 500$ is used to compute $\hat{D}_1$, y_i $\forall i = 501, 502, \ldots, 1000$ is used to compute $\hat{D}_2$, and y_i $\forall i = 1001, 1002, \ldots, 1500$ is used to compute $\hat{D}_3$.

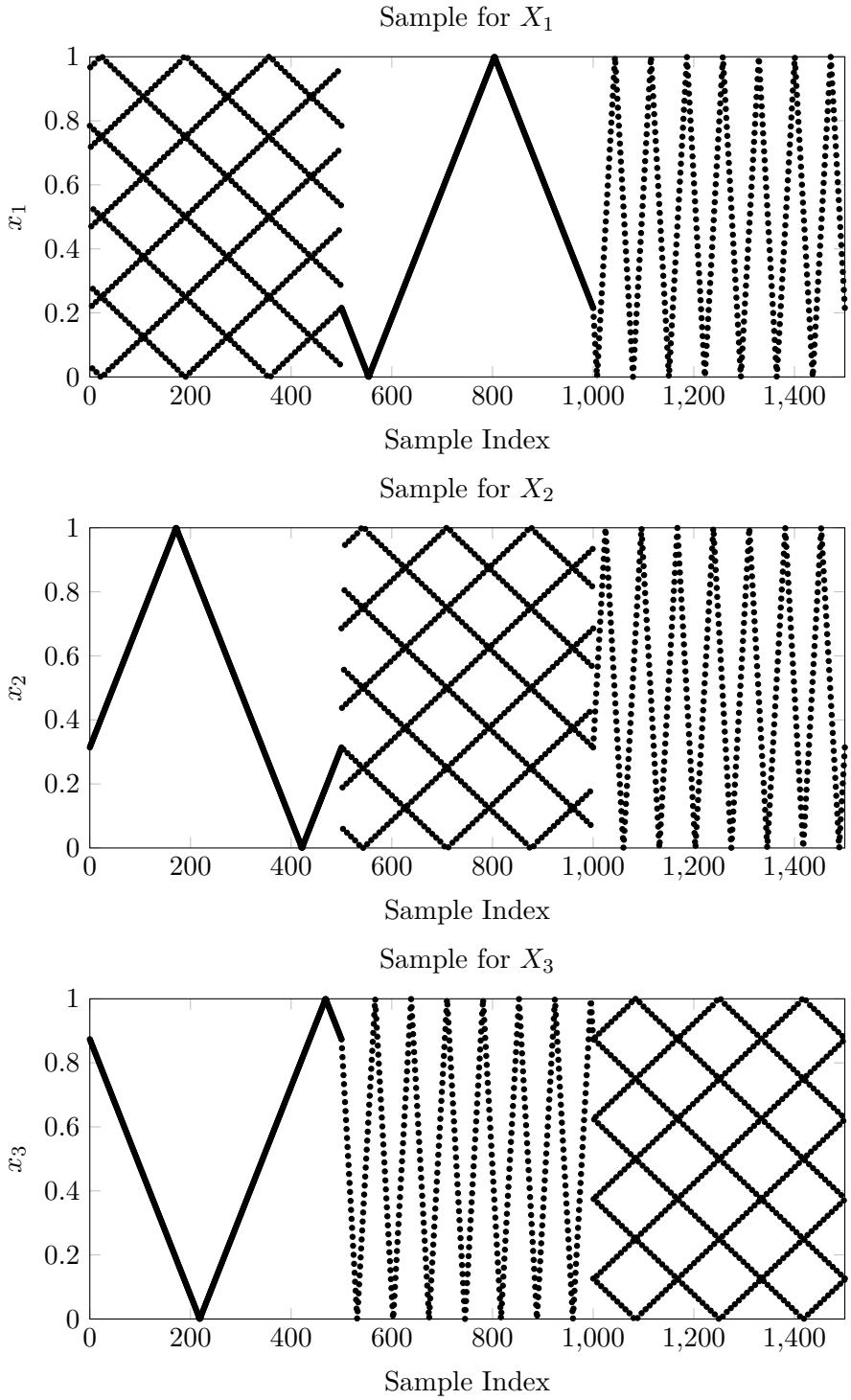

Fig. 2.3: Distribution of samples for three variables x_i computed using equation 2.48. Due to the loss of symmetry using the eFAST method the computation of the partial variances for each variable needs its own sample space.

2.2.3.2 Total Indices

The idea of Total Indices was proposed in (Saltelli et al., 1999) as an extension of the FAST method. The so far neglected frequencies, that do not belong to the set $p_i\,\omega_i$, $\forall i = 1, 2, \ldots, n$, $\forall\, p_i = 1, 2, \ldots, \infty$, do not account for the Variance of the output. To access this residual Variance a set in the form $p\,\omega_{-i}$, with $-i$ representing "all but i" is defined. The estimation of the variance D_{-i} is then computed as

$$\hat{D}_{-i} = 2\sum_{p=1}^{\infty}(A^2_{p,\omega_{-i}} + B^2_{p,\omega_{-i}})\,. \tag{2.49}$$

$\hat{D}_{-i}/D$ then represents all effects of any order, which are not consequences of x_i. Therefore, $1 - \hat{D}_{-i}/D$ represent all effects which are consequences of x_i. This is referred to as the total Sensitivity Indices $S_{i,T}$ (Chan et al., 2000).

2.2.4 Two Sample Test

Two Sample Test, or Segmentation based methods (Hagentoft et al., 2015), revolve around the idea of applying tests of goodness of fit to two sets of random samples. Initially these tests intended to test if the distribution of a random sample fits a known, specified distribution. In the context of SA the tests are used differently. The general idea is to take a subset of the models output, and test it against the rest of the output. In this case the models output is divided into a bottom and a top set, with the median as the divider. The Segmentation is shown in Fig. 2.4 using $F(y)$, the cumulative distribution function of the model output y.

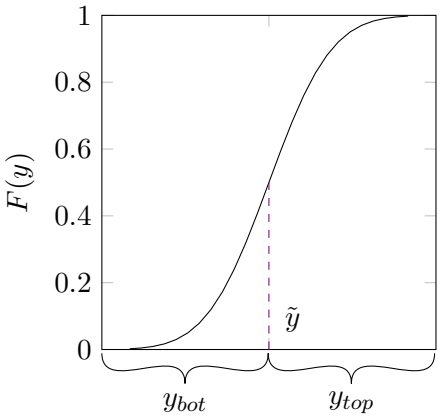

Fig. 2.4: Segmentation of the model output into two parts, top and bottom, using the median of the model output as a divider.

The two set tests are now utilized to compare the distribution of the variable x_i in both the y_{top} and y_{bot} set. In other words, we are interested in $F(x_i \,|\, y(x_i) \in y_{bot})$ and $F(x_i \,|\, y(x_i) \in y_{top})$. To these distributions the Kolmogerov-Smirnov test is applied

$$S_i = \sup\left[|F(x_i \,|\, y(x_i) \in y_{top}) - F(x_i \,|\, y(x_i) \in y_{bot})|\right]\,. \tag{2.50}$$

More information on the test can be found in (Conover, 1980). The test statistic S_i, which in the intended way would be used to reject or confirm the hypotheses, is now used as a Sensitivity Index. The drawn conclusion is, that if $F(x_i \,|\, y(x_i) \in y_{bot})$ and $F(x_i \,|\, y(x_i) \in y_{top})$ share a similar distribution, x_i has little impact on y. Analoguesly, if the distributions differ, x_i has a greater impact on y. An illustration of these two cases is shown in Fig. 2.5.

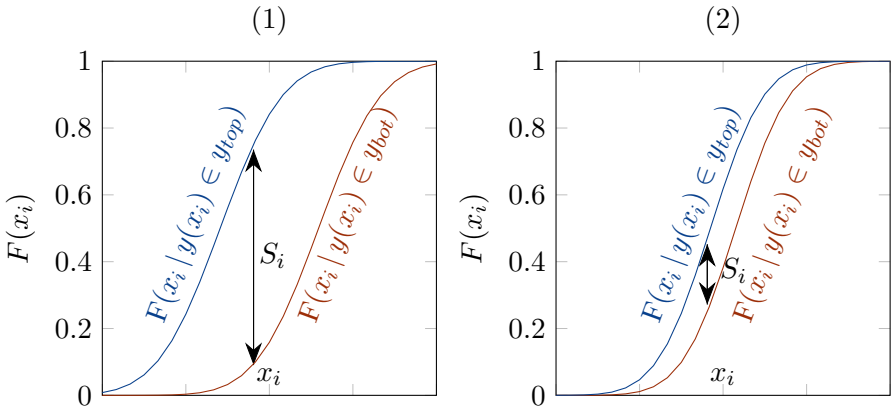

Fig. 2.5: High (1) and low (2) sensitivity S_i of the model output y in respect to the variable i as an interpretation of the similiarity between $F(x_i \,|\, y(x_i) \in y_{bot})$ and $F(x_i \,|\, y(x_i) \in y_{top})$ quantified through the Kolmogorov-Smirnov test.

2.2.4.1 Sampling

Unlike in the FAST method, segmentation based methods are not restricted to certain kind of sampling. To ensure a full coverage of the sampling space different methods have been developed. In this work the segmentation based analysis, is sampled using the LHC method, developed in (McKay et al., 1979). Instead of sampling purely random in the sample space, the sample space is divided into n segments of equal probability, where n is also the number of samples. From each of these segments then random tuples are picked without replacement. Which segments are paired between the variables is random, but each variable's segment is represented exactly once. A comparison between LHC sampling and random sampling is shown in Fig. 2.6.

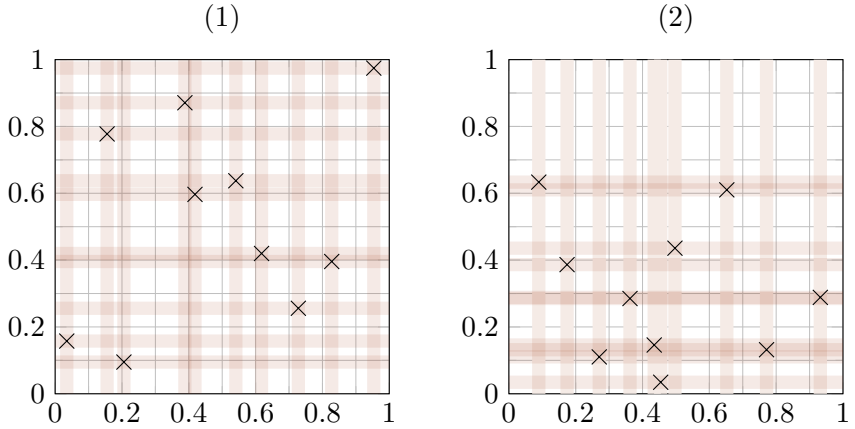

Fig. 2.6: Comparision of random samples in two variables of a sample size N=10 using LHC (1) and random sampling (2), with horizontal and vertical lines indicating the coverage of the sample space.

2.3 Confidence

All the so far mentioned results of the simulation are estimates. This applies to the mean and standard deviation of the physical quantities, but also to the Sensitivity Indices for the random variables. An approach to quantify the accuracy of these estimates is through confidence intervals. As an example, an experiment using the model $y = f(x_1, x_2, ..., x_k)$, with the random variables x_i is done for n samples in x_i. After an estimation for the mean of the model output $\overline{\mathbf{y}}(y_1, y_2, ..., y_n)$ is computed, we are now interested in how good the estimate for the mean fits the mean of the population of $\mathbf{y}$. One approach to this is *Bootstrapping*, a computational method to estimate the standard error of a estimated paramter $\hat{\theta} = t(y)$ based on the sample $\mathbf{y}$, first discussed in (Efron, 1992). This is achieved by resampling the sample, in this case with replacement. The sample, resulting from the estimated paramter for each resampled sample, then allows to estimate the standard error of the estimated parameter. In (Archer et al., 1997) this is discussed in the context of Sensitivity Indices computed using the fast method. In (Efron and Tibshirani, 1994) the general approach is explained. We assume the experiment has yielded n outputs $y_1, y_2, ..., y_n$ on which a statistic is to be computed on. The method itself takes place in three steps, described in (Efron and Tibshirani, 1994) as:

1. Take an independent bootstrap sample y_i^* of n samples from $y_1, y_2, ..., y_n$ with replacing.
2. Compute the estimate for the bootstrap mean $\mathbf{y}_k^*$ from the set $y_1^*, y_2^*, ..., y_n^*$.
3. Repeat step one and two, until a sufficient size for distribution $\overline{\mathbf{y}}$ is created, and compute the standard error $SE(\overline{\mathbf{y}})$.

Even tough the population of y does not follow a normal distribution, $\overline{\mathbf{y}}$ will follow a distribution similar to the normal distribution. This assumption allows computing the confidence intervals using the standard error $SE(\overline{\mathbf{y}})$ and the percentile intervals of the normal distribution. For a confidence of 90% it yields

$$\overline{y} \pm 1.645\, SE(\overline{\mathbf{y}})\,. \tag{2.51}$$

As $\overline{\mathbf{y}}$ does not necessarily follow a normal distribution, this is just an approximation of the confidence interval. *Non-parametric* methods, which follow a more advanced scheme, can be found in (Efron and Tibshirani, 1994).

Efron and Tibshirani (1994) suggest 200 resamples can be sufficient for the bootstrapped standard error, Archer et al. (1997) suggest that 1000 or 2000 numbers of resampling can be sufficient for the estimation of the confidence intervals of Sensitivity Indices. Concluding a short example is made to illustrate the method. Let y follow an exponential distribution with an expected value of $\mu = 1$ and a variance $Var(y) = 1$

$$f_Y(y) = e^{-y} \tag{2.52}$$

Now an in the probability space equally distributed (to ensure this LHC sampling is used) sample $\mathbf{y} = y_1, y_2, ..., y_n$, with $n = 200$ is sampled and an arithmetic mean $\overline{y}$ is calculated as the estimator for μ. An illustration of the probability density function and the distribution of the sample is shown in Fig. 2.7.

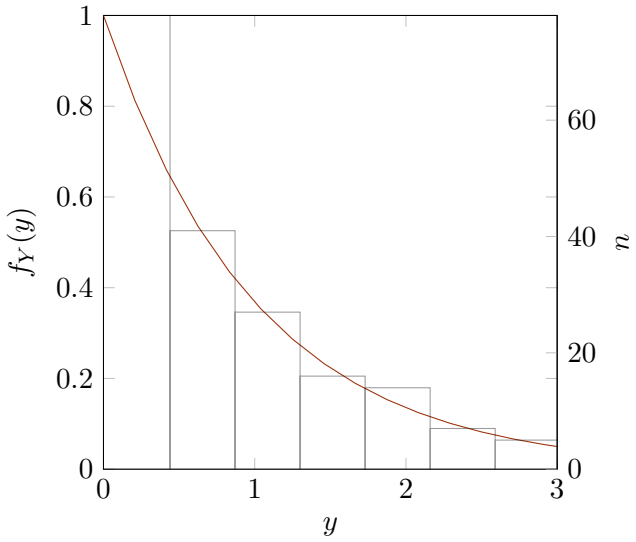

Fig. 2.7: Probability density function $f(y)$ and a histogram of the discrete propability distribution of the sample $\mathbf{y}$.

From this sample a bootstrap sample in the form $\mathbf{y}^* = y_1^*, y_2^*, ..., y_n^*$ is sampled with replacement, $k = 200$ times. From each of the bootstrap samples the arithmetic mean is computed yielding $\overline{\mathbf{y}}^* = \overline{y}_1^*, \overline{y}_2^*, ..., \overline{y}_k^*$. The 90% confidence interval can then be computed as

$$[\overline{y} + 1.645\, SE(\overline{\mathbf{y}}), \overline{y} - 1.645\, SE(\overline{\mathbf{y}})] \tag{2.53}$$

A histogram of the arithmetic means of the bootstrap samples $\overline{\mathbf{y}}^*$, including the estimate for the expected value $\overline{y}$, and the estimated confidence interval C_i is shown in Fig. 2.8.

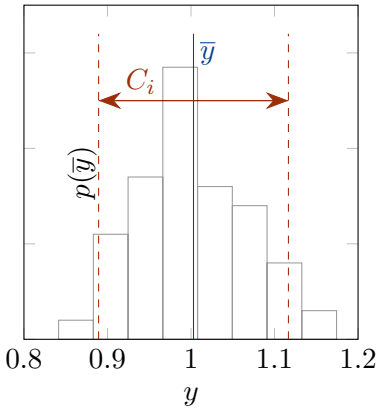

Fig. 2.8: Histogram of the aritmetic means of the 200 boostrap samples $\overline{\mathbf{y}}^*$ including the estimate for the expected value $\overline{y}$ and the estimated confidence interval C_i.

Chapter 3

Software Architecture

This Chapter revolves around the implementation of the methods discussed in Chapter 2. At first, a simulation framework, which extends the Ham4D hygrothermal simulation software to allow for probabilistic simulations is presented. It is discussed what changes are introduced to the input and output and which programming languages are chosen. With the framework established, the introduced pre- and post-processing units, and their respective in- and outputs are described. Concluding the chapter the implementations of the in Sec. 2.2 presented methods are discussed.

3.1 Simulation Framework

To apply SA in combination with the hygrothermal simulation software Ham4D, a new simulation Framework is developed. At the current state, Ham4D only allows for deterministic simulations. To create a toolkit, which follows a probabilistic approach, Ham4D is wrapped by pre- and post-processing units. Such a Framework is illustrated in Fig. 3.1.

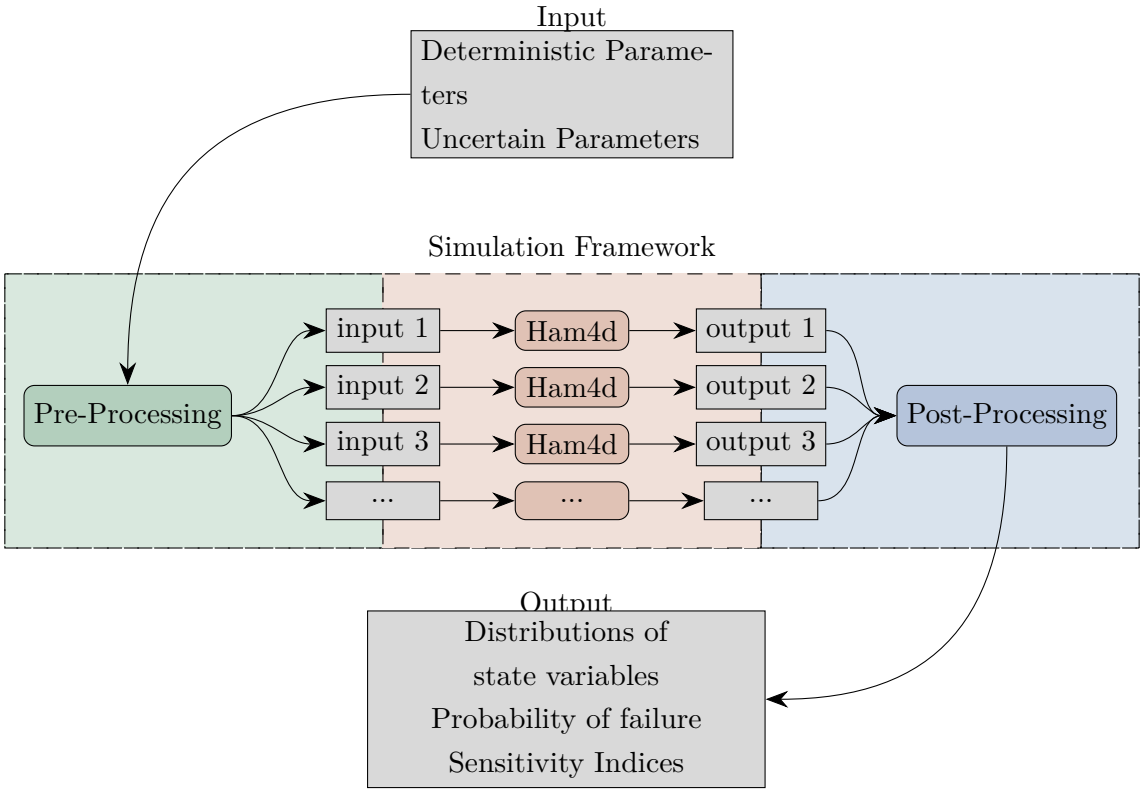

Fig. 3.1: Structure of simulation framework allowing for probabilistic simulations using Ham4d.

In this case, pre-processing deals with the preparation of the input files. The input to the framework are deterministic parameters, uncertainty parameters and sample parameters. The uncertainty parameters include information on the distribution parameters, usually the expected value and the standard deviation. From the sample parameters, the pre-processing unit then generates a sample set in the K space using the sample methods discussed in Sec. 2.2.3.1 and Sec. 2.2.4.1. The generated sample is applied to the cumulative distributions of the uncertain input parameters. Finally, the input files are populated with both the deterministic and uncertain input parameters. The pre-processing unit is written in python, as it

- works on tasks of low computational effort,
- requires access to sampling and stochastic libraries,
- should allow for adaptions by a wide range of users.

The structure of the pre-processing unit and how input data is processed, resulting in the Ham4D input files is shown in Fig. 3.2.

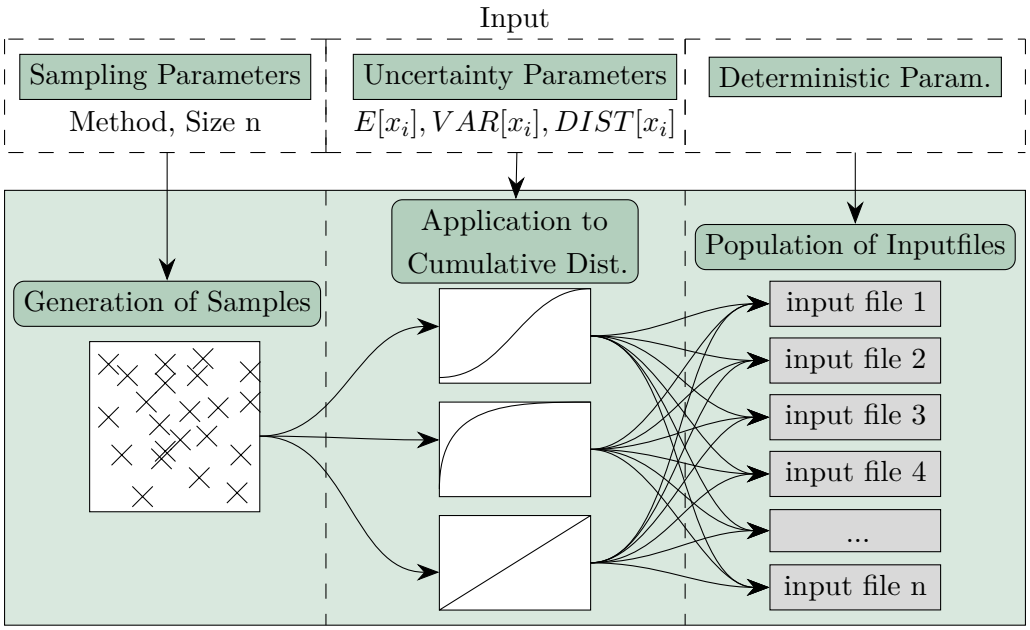

Fig. 3.2: Structure of the pre-processing, structure of the input data, and processing of the input data in sub-tasks.

With the n input files generated, Ham4D can be instructed as before to compute the n output files. Each output file contains the propagated state variables for each time step and information on the problem needed to reconstruct the mesh. Even though the latter being repeated in each output file, its size is insignificant to the size of the stored state variables.

The post-processing unit then reads the output files time step by time step. As the state variables are stored in order of cells, they are transposed to increase performance in stochastic analysis. Additionally, homogenized field variables are computed. In contradiction to the name, field variables only contain one value for the whole domain. The transposed state variables and the field variables are the data structures, which the stochastic analysis are then performed on. In the *Estimate Population* step the mean and the standard deviation are estimated. In *Risk Analysis* the sample is tested against the defined failure criteria resulting in probabilities of failure. In the *Sensitivity Analysis* step the sample is analysed using the methods discussed in Sec. 2.2.3.2 and Sec. 2.2.4 to estimate the input output relation. This results, depending on the chosen method, in one or two Sensitivity Indices per uncertain input parameter. As all the above-mentioned results are estimations and therefore subject to uncertainty themselves, a *Reliability Analysis* is performed. In this step, a confidence interval for each of the results is estimated through the bootstrapping method discussed in Sec. 2.3. Finalizing the post-processing, the output is parsed using the VTK-library (Schroeder et al., 2006) to allow for visualization of the simulation results, resulting in a `.vtu` file for each time step. The post-processing unit is written in C++ as

- especialliy the FAST method has a high computational effort,
- it simplifies future implementation in Ham4D, which is written in C++.

The structure of the post-processing unit and how output files are processed is shown in Fig. 3.2.

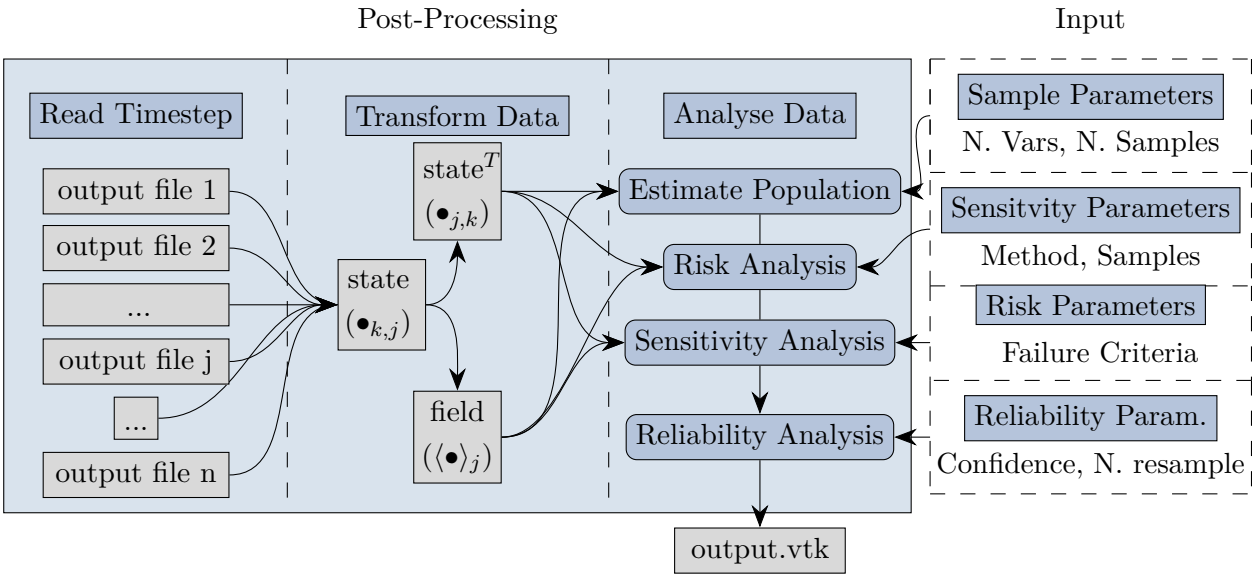

Fig. 3.3: Structure of the post-processing, structure of the input data, and processing of the input data in sub-tasks.

The output of the proposed framework now holds all the information gained through the probabilistic approach. Where the deterministic output held only the state variables for each time step, the probabilistic output now holds the mean value, the standard deviation, one or two Sensitivity Indices for each uncertain input parameter, probabilities of failure for each failure criterion and for each of these respective confidence intervals. An example of this data structure, for a single cell and a single state variable $\bullet$, is illustrated in Fig. 3.4.

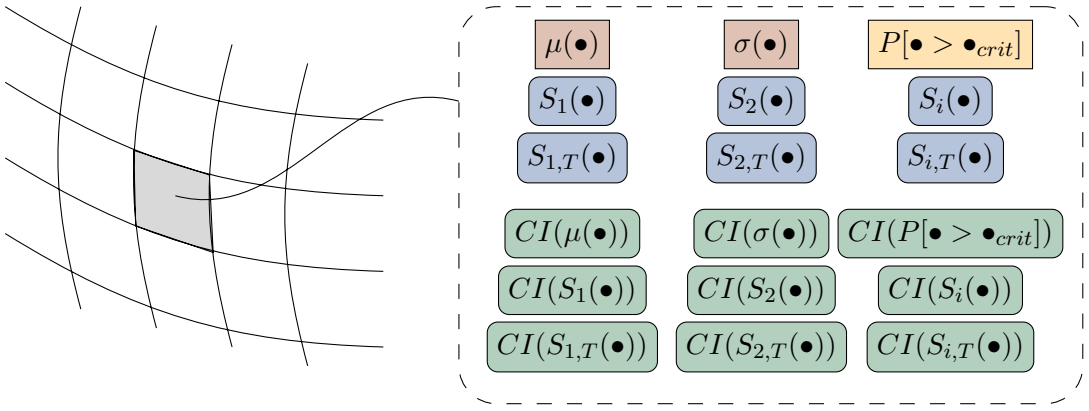

Fig. 3.4: Structure of the results of the framework held in a cell for a single state variable $\bullet$.

3.2 Implementation of Sensitivity Analysis Methods

Concluding this chapter we want to shortly discuss the implementations of the Sensitivity Analysis Methods used in this work. The post-processing library is written in C++, therefore available C or C++ libraries providing the needed methods are used.

3.2.1 Fourier Amplitude Sensitivity Test

At the date of this work no C or C++ library containing the FAST or eFAST algorithms were found. Therefore, the algorithms were implemented, heavily guided by the implementation provided in SALib, an open-source Python library (Herman and Usher, 2017). The implementation in this library is based on the R package *fast99* written by Gilles Pujol 2006 (Iooss et al., 2006).

The implementation in this work differs from the one in (Herman and Usher, 2017) in the form, that the confidence intervals are estimated through bootstrapping the whole data instead of half the data. This is done to ensure comperability between the SA methods.

For the Fourier transformation itself the C library FFTW3 developed in (Frigo and Johnson, 2005) is used.

3.2.2 Segmentation Based Method

For the segmentation based method no applicable library was found. Therefore, a new algorithm for the method was developed. To document how the sensitivity is computed, it is shortly presented here.

As a simplification, the problem is reduced to an output vector $\mathbf{y}$ containing $i = 1, ..., n$ values, with $y_i(x_i)$ the model output of the sample x_i. In this simplified case $\mathbf{y}$ is only subject to one random variable, x_i is therefore a scalar value. In addition to the output vector, the sample vector $\mathbf{x}$ is stored.

At the starting point both the vector $\mathbf{y}$ and the vector $\mathbf{x}$ are not sorted and follow the index $i = 1, ..., n$. In the first step the $\mathbf{y}$ vector is sorted by $\mathbf{x}$ and re-indexed using the index $j = 1, ..., n$. Rising index j therefore resembles a rising variable x. Then the $\mathbf{y}$ vector is sorted, allowing to split the output by the median as shown in Fig. 2.4. The resulting vector is indexed using the index $k = 1, ..., n$. Now a new vector F of size n holding zeros is constructed. This vector will resemble the cumulative distribution $F(x_i \,|\, y(x_i) \in y_{bot}) - F(x_i \,|\, y(x_i) \in y_{top})$.

In the next step F is filled by looping over the bottom set of the sorted output vector y_{bot} (index k) and incrementing the element F_j^{bot} and all elements above by one. The subtraction $F^{bot} - F^{top}$ is then achieved through looping over the sorted output vector y_{top} (index k) and decrementing the element F_j^{bot} and all elements above by one. Now the maximum of the absolute difference between the two distribution is computed as $max(|F|)$ and finally, the sensitivity is normed as $S = max(|F|)\, 2/n$. A pseudo code of this is shown in Lst. 3.1.

When applying this method on the initial complexity, it is advisable to implement the first sort to happen before looping over the cells.

Listing 3.1 Segmentation Based Method

```
segmentation_based_method(y,x){
    y.sort_by(x);

    vector<tuple<double,int> y_indexed = {0,y.size};

    for j in 0 ... y.size()-1
        y.first = y[j];
        y.second = j;

    vector F = {y.size(),0}

    for m in 0 ... y_dash.size/2
        j = y_dash.second[m];
        for l in j ... y_dash.second/2
            F[l] += 1;

    for m in (y_dash.size+1)/2 ... y_dash.size-1
        j = y_dash.second[m];
        for l in j ... y_dash.second/2;
            F[l] -= 1;

    S = max(abs(F))/n;

    return S;
}
```

Chapter 4

CaseStudy

Having explored possible methods to further analyse hygrothermal aspects of building components in Chapter 2, and its implementation in Chapter 3, testing the methods through application to specific cases is of interest.

This section deals with the application and interpretation of these methods on cases, with rising complexity.

The first example (Sec. 4.1) a two-dimensional, initial value, thermal conduction problem is analysed. The aim of this example, is to analyse three properties of SA on the basis of a comprehensible and predictable problem. At first, we want to test the capabilities of SA in relating local effect in the state variables to uncertain material properties. Secondly, the differences in Sensitivity Indices and partial variances are investigated. Finally, the time dependent behaviour of the Sensitivity Indices and the partial variances is investigated.

In the second example (Sec. 4.2) the context of building science is added. With this, the complexity is increased to a coupled heat and moisture problem. In this example the convergence behaviour of the SA method is investigated. This is achieved through inspection of the respective confidence intervals for different sample sizes and through comparison of the Sensitivity Indices for different sample sizes. The aim is to investigate if the confidence intervals are able to indicate how far the Sensitivity Indices have converged. Additionally, it is tested if the models converge to the same Sensitivity Indices. Lastly, it is tested if the segmentation based method is applicable to samples, generated using the search curve method.

In the third example (Sec. 4.3), the problem is expanded to include convective heat and moisture transport. In this example we want to investigate the capabilities of SA, as a tool used in decision-making. Therefore, a failing construction is analysed, with the aim to identify relevant parameters and guide the analyst in the decision-making, as how to reduce the failure probability. This is tested on a low sample size, to ensure a reasonable computational effort.

All simulations are run on single units, and should take no more than 8 hours to finish. This should allow analysts to simulate the problems overnight.

4.1 Behaviour of Sensitivity Indices using the example of Conductive Heat Transport

In the first case a two-dimensional initial value problem is analyzed. The domain consists of three materials, two of which, in the further named material A and material B, are subject to an uncertainty in the form of a normal distributed thermal conductivity. The third material, material C, shows a deterministic thermal conductivity significantly lower than those of material A and material B. The domain is constantly heated on one side, modelled as a Dirichlet boundary condition. The geometric setup of the construction and relevant material parameters are illustrated in Fig. 4.1. All additional parameters used in the simulation can be found in Sec. A.1.1.

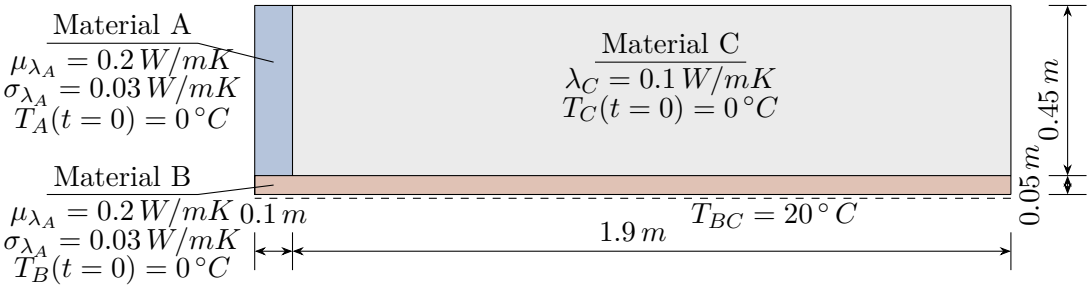

Fig. 4.1: Set up of the two-dimensional initial value problem consisting of three materials A, B and C, with material A and B showing uncertain heat conductivity. The domain has three adiabatic boundaries and a constant temperature boundary on one side.

The domain is uniformly meshed through squares with side lengths $a = 0.05\,\mathrm{m}$. The mesh is shown in Fig. 4.2.

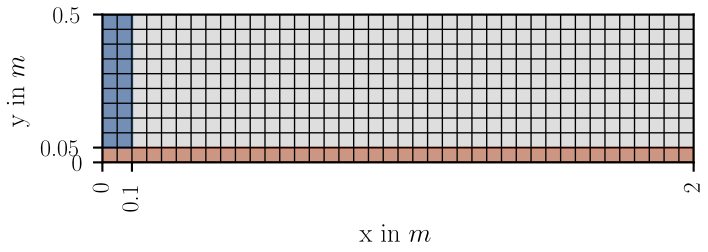

Fig. 4.2: Finite volume mesh of the initial value problem

The case is analysed using the eFAST method described in Sec. 2.2.3. A sample of size $N = 130$ (λ_A, λ_B) is generated using the interference factor $M = 4$. The frequencies $\omega = \{16, 1\}$ are chosen by applying the eFAST algorithm discussed in (Saltelli et al., 1999). The estimation for the expected value and standard deviation of T at the time steps $t = 1, 10, 20, 30\,\mathrm{h}$ are shown in Fig. 4.3. The respective widths of the confidence intervals can be found in Fig. A.1.

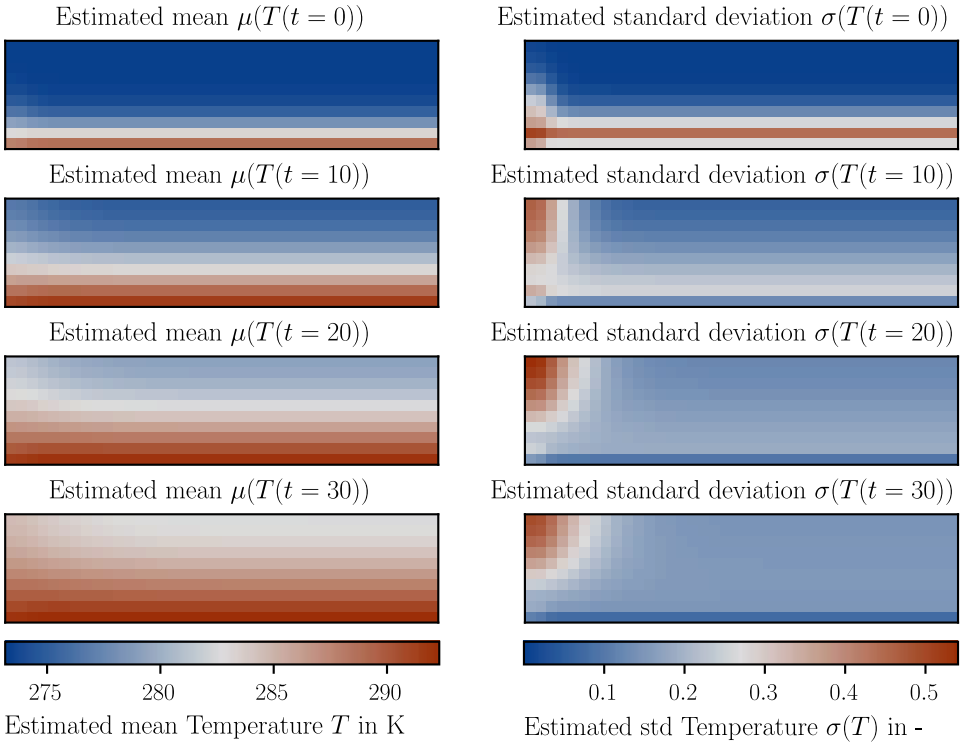

Fig. 4.3: Estimated mean $\mu(T)$ and standard deviation $\sigma(T)$ of the temperature field, at the timesteps $t = 1, 10, 20, 30\,\text{h}$, showing assymetric fields and localized variation in the temperaturefield due to the uncertainty in the material parameters (λ_A, λ_B).

Experience suggests, that the asymmetric temperature field is a result of the differing thermal conductivity in the materials A and C, rather than the differing thermal conductivity in materials B and C. SA now provides a possibility to quantify this relation. Inspection of the Sensitivity Indices allows assigning local variation in the fields to the uncertain variables λ_A, λ_B. Fig. 4.4 shows that the impact of λ_B is concentrated on the left side of the domain, expanding to the right with as the simulation progresses. The respective widths of the confidence intervals can be found in Fig. A.2.

The Sensitivity Indices in Fig. 4.4 are of higher order, they therefore not only include the direct effects but also the interactive effects. Specialisation of Eq. 2.49 for the two uncertain variables A and B, and division by the variance D results in

$$S_{A,T} = 1 - S_{-A} = 1 - S_B \tag{4.1}$$

and

$$S_{B,T} = 1 - S_{-B} = 1 - S_A\,. \tag{4.2}$$

Through evaluation of the sum

$$S_{A,T} + S_{B,T} = 1 + 1 - \sum_{i}^{A,B} S_i = 1 + S_{AB} \tag{4.3}$$

it becomes apparent that $S_{A,T} + S_{B,T} \neq 1$. Therefore, If the sum of the total Sensitivity Indices exceeds 1, this indicates interactive effects between the uncertain variables. In the case of Fig. 4.4 no interactive effects, exceeding the confidence intervals, can be identified.

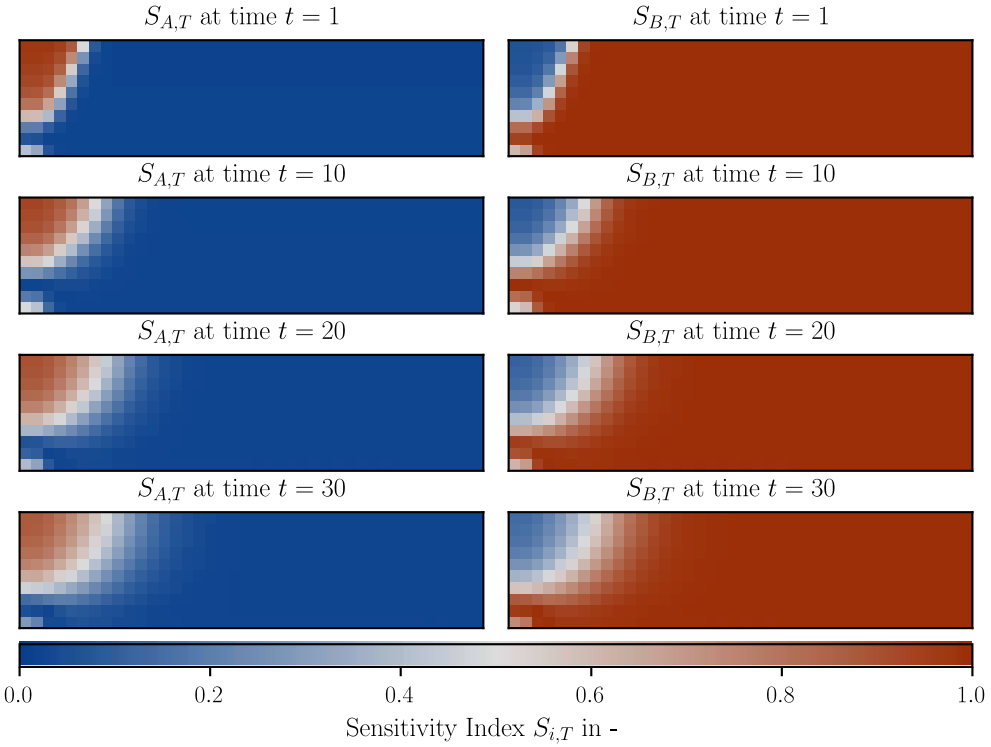

Fig. 4.4: Total Sensitivity Indices $S_{i,T}$ for a sample size N=130, at the timesteps $t = 1, 10, 20, 30$ h, indicating the sensitivity of the temperature field in respect to the heat conductivities λ_A and λ_B.

Upon inspection, the Sensitivity Indices do not provide information on the variation itself. Thus, it can be of interest to compute the partial variances $\hat{D}_i$ as

$$\hat{D}_i = S_{i,T}\, D = S_{i,T}\, \sigma(T)^2\,, \tag{4.4}$$

to ensure inspected sensitivities are results of substantial variance. The resulting partial variance fields are shown in Fig. 4.5. This can be of relevance when inspecting the sensitivity of a field, as high sensitivities can create the impression of a great impact of a variable, even though the partial variances are actually small.

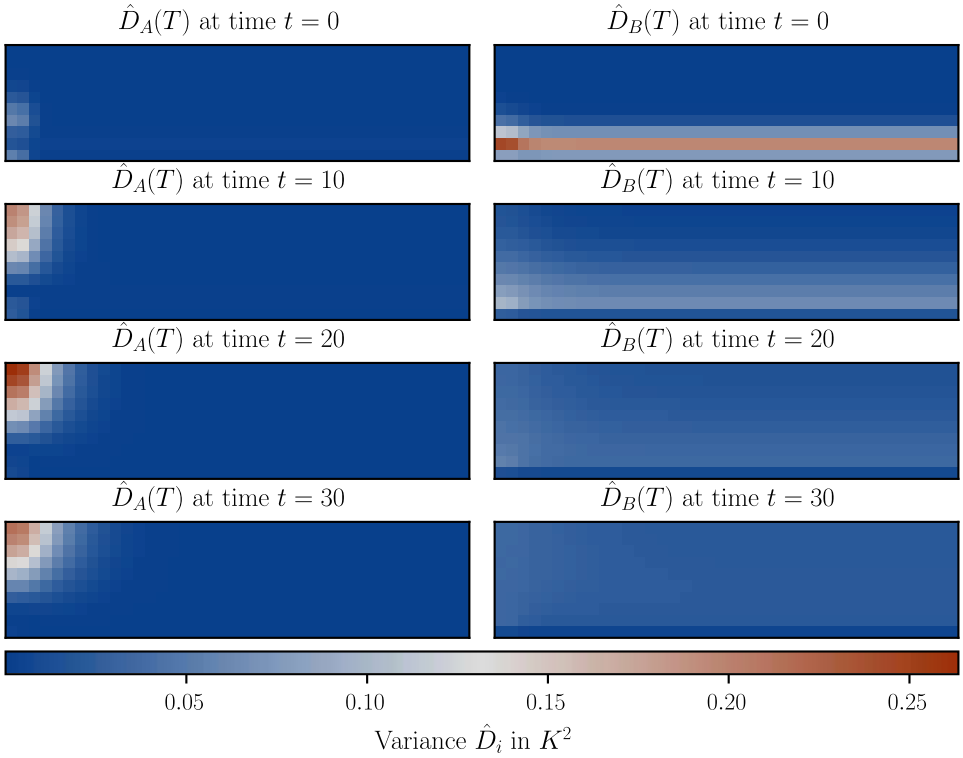

Fig. 4.5: Partial variance of the temperature field $\hat{D}_A(T)$ and $\hat{D}_B(T)$ as a result of the varying heat conductivities λ_A and λ_B, computed using the extended FAST method.

For some criterion in evaluation it can be of interest to analyse a homogenized field variable. Applying volumetric homogenization of the field variables as

$$\langle \bullet \rangle = \frac{1}{V} \int_V \bullet \, dx \tag{4.5}$$

and further applying SA allows for an analysis of effect of the random variables on the homogenized variable. Returning to the differing behaviour of sensitivity and partial variances, the time dependent behaviour of the partial variances of the homogenized temperature and the Sensitivity Indices in regard to the homogenized temperature show significantly different behaviour, Fig. 4.6. While the partial variances converge to zero once the whole domain reaches the temperature of the boundary condition, the Sensitivity Indices stabilize. This indicates, that the variance of homogenized temperature converges with a similar rate as the partial variances.

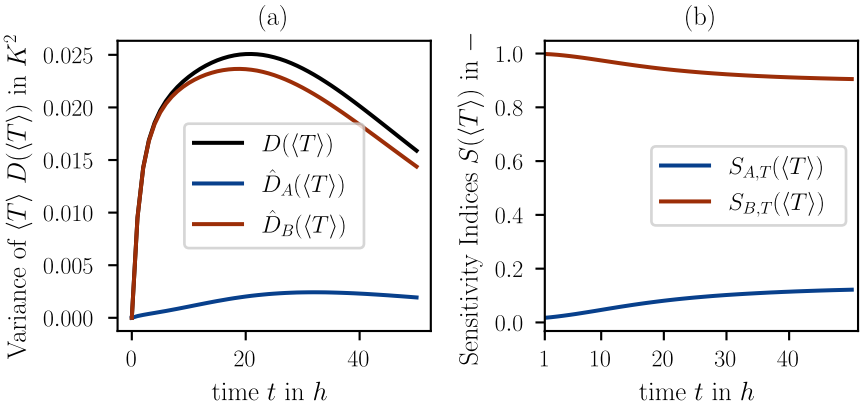

Fig. 4.6: The time dependent behaviour of the partial variances $\hat{D}_i(\langle T \rangle)$ (a) and the Sensitivity Indices $S_{i,T}(\langle T \rangle)$ (b) of the homogenized temperature in respect to the varying heat conductivities λ_A and λ_B.

4.2 Convergence of Sensitivity Indices at the example of diffusive moisture transport in flat roofs

With the general behaviour of Sensitivity Indices established, the complexity of the problem is increased to closer resemble a realistic building component. In this example a simplified flat roof exposed to realistic climate conditions is analysed. The domain consists of two oak boards with blow-in cellulose insulation in between. The component is subject to uncertainties in the form of the s_d-value of the vapour barrier and the s_d-value of the roof sealing. The setup of the problem is illustrated in Fig. 4.7. The exterior climate is created using open climate data provided by (Zentralanstalt für Meteorologie und Geodynamik, 2023). The interior climate is derived from the exterior climate according to ("ÖNORM B 8110-2:2020-01," 2020). The used boundary conditions, as well as the used material data can be found in Sec. A.1.2.

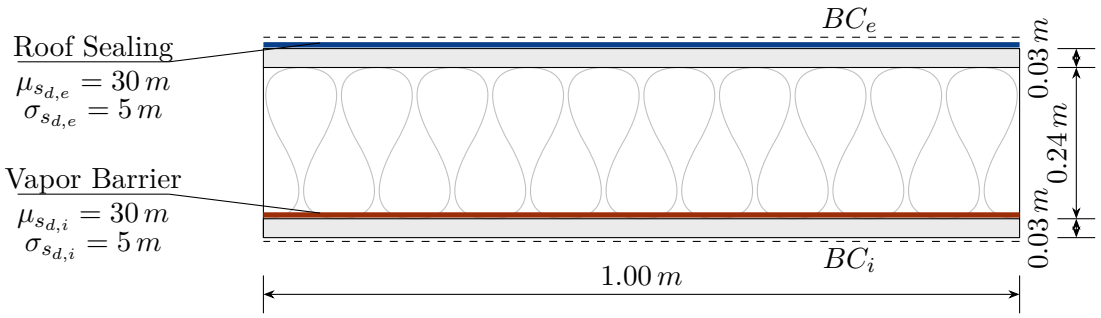

Fig. 4.7: Set up of the one-dimensional flat roof problem consisting of two uncertain input parameters, the s_d-value of the interior vapour barrier $s_{d,i}$ and the s_d-value of the exterior roof sealing $s_{d,e}$. The domain has two adiabatic boundaries and boundary conditions resembling realistic indoor and outdoor climate.

The example is modelled as a one dimensional problem, using the mesh depicted in Fig. 4.8. The domain is uniformly meshed through cells with height $h = 0.03\,\mathrm{m}$. The problem is simulated for a duration of 5 years.

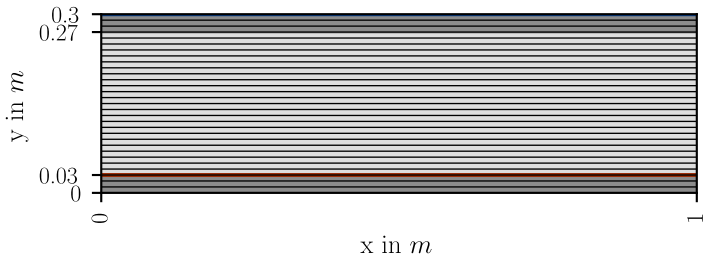

Fig. 4.8: Finite-Volume mesh of the flat roof problem with uniform cell heights $h = 0.03\,\mathrm{m}$.

In this example we want to explore the convergence behaviour of the FAST and the segmentation based method. Therefore, the simulation is run once with $N = \{130, 160, 520\}$ for each method, using LHC sampling for the samples used in the segmentation based SA method. For the eFAST method the interference factor $M = 4$, and the frequencies $\omega = \{(1, 8), (1, 16), (1, 32)\}$ are chosen. Before exploring the Sensitivity Indices we want to discuss the global behaviour of the problem. The propagation of the homogenized moisture content $\langle w \rangle$ suggests that the construction is expected to dry out the initial moisture content in the first simulation year, with an indication of rising trend in the last simulation years. As depicted in Fig. 4.9, the data shows significant variation in the moisture content in the later years.

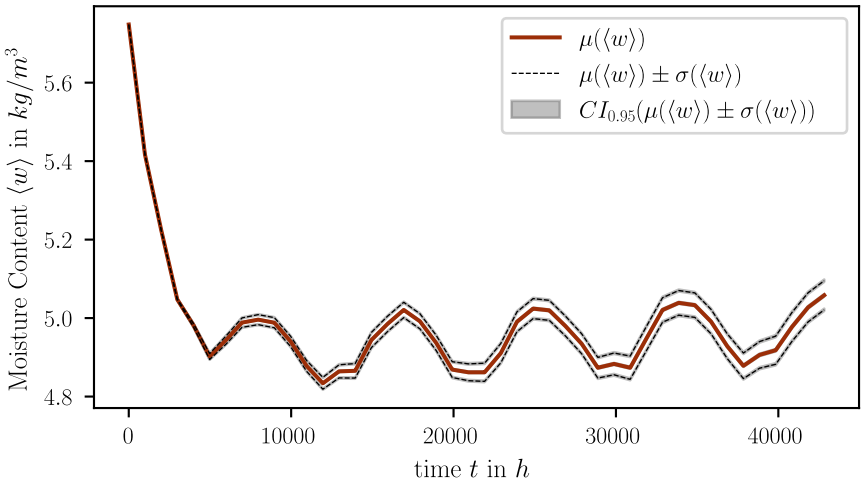

Fig. 4.9: Homogenized moisture content in the flat roof construction evaluated for a sample size $N = 520$. Both sampling methods (FAST and LHC) provide equivilant results.

Inspection of the homogenized partial variances shows, that even though the confidence in the standard deviation and mean estimators is high, the confidence is significantly lower for the variances and the sensitivities. The Sensitivity indices in Fig. 4.10 shows both periodic and

non periodic time dependent behaviour. In the first year, when the initial moisture is drying, the sensitivities invert and in the later years the impact of the s_d-value of the roof sealing rises. An interpretation of this is that the moisture inside the upper oak boarding manly dries to the exterior, as this process is dominated by the s_d-value of the roof sealing, its impact rises with moisture accumulating in the oak boarding. This is further supported by the periodic behaviour, as in the yearly drying periods, the sensitivity of the homogenized moisture content in respect to the s_d-value of the roof sealing is higher. Analogous, in the wetting periods the moisture load due to the indoor climate is higher, resulting in higher sensitivities of the homogenized moisture content in respect to the s_d-value of the vapour barrier.

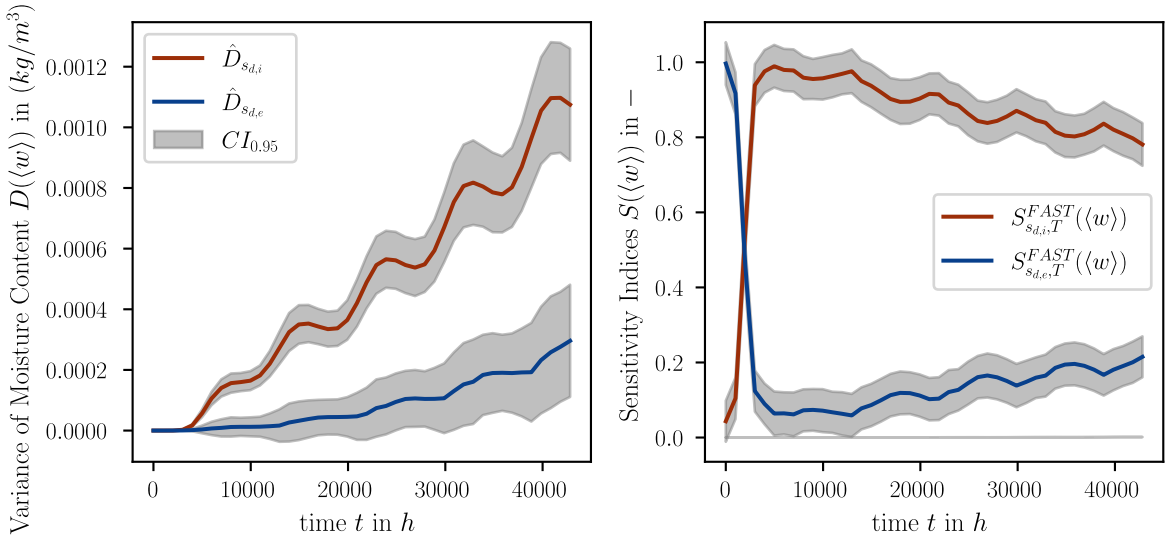

Fig. 4.10: The time dependent behaviour of the partial variances $\hat{D}_i(\langle w \rangle)$ (left) and the Sensitivity Indices $S_{i,T}(\langle w \rangle)$ (right) of the homogenized moisture in a flat roof, in respect to the varying s_d-values of the interior vapour barrier $s_{d,i}$ and the exterior roof sealing $s_{d,e}$. Computed using the extended FAST method with sample size $N = 520$.

Comparison of the Sensitivity Indices computed for different sample sizes and methods at a winter day in the last simulation year ($t = 39840\,h$), shows that both methods predict a similar model behaviour, with the segmentation based method estimating lower sensitivities. The s_d-value of the vapour barrier dominates in the interior oriented strand board and the blow-in cellulose insulation. In the upper oriented strand board both the s_d-value of the roof sealing and the s_d-value of the vapour barrier show significant impact.

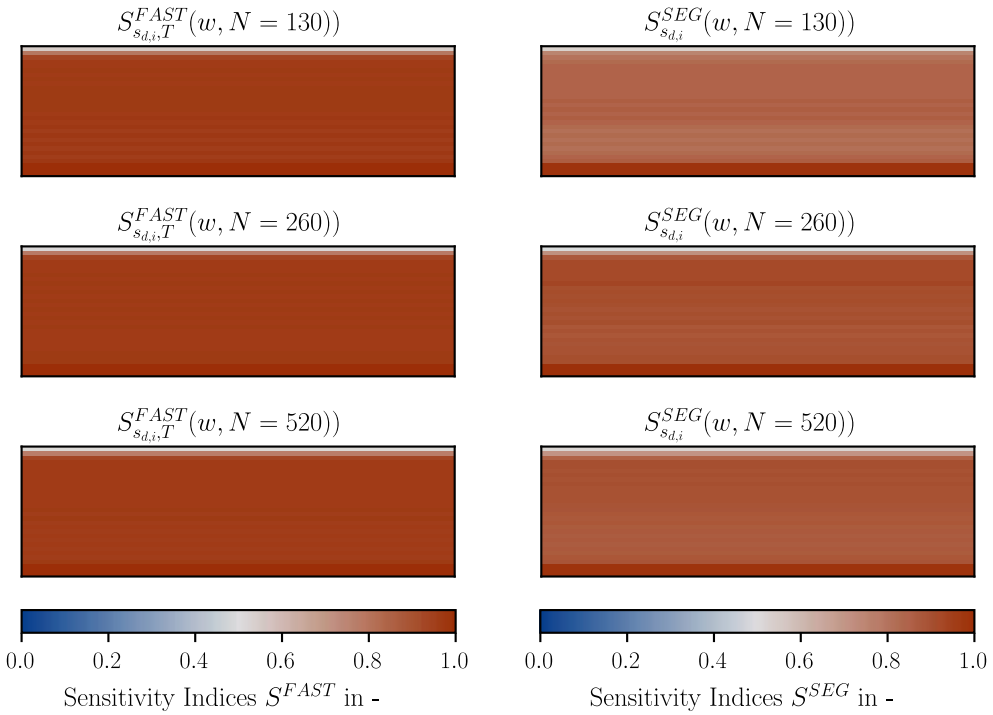

Fig. 4.11: Comparision of Sensitivity Indices S using the FAST method (left) and the segmentation based method (right), for the sample sizes $N = 130, 260, 520$, on a winter day in the last simulation year ($t = 39840\,h$).

Turning to the convergence behaviour of the sensitivity indices, measured by the widths of the confidence intervals, it becomes apparent that the methods show significant differences. Sensitivity Indices computed using the FAST method show confidence intervals independent of the sensitivity itself. This leads to homogenous confidences in the whole domain, as depicted in Fig. 4.12, and the levels of confidence shown in Fig. 4.13. Whereas the Sensitivity Indices computed using the segmentation based method show confidence intervals dependent of the sensitivity itself. Therefore, in Fig. 4.12 the different sensitivities in the oak boarding become visible in the confidence field and Fig. 4.13 shows parabolic behaviour with low confidences for medium sensitivities and high confidences for very low and very high sensitivities.

The level like behaviour of the confidences for the FAST sensitivities, suggest, that computation of the confidence in fever cells could be sufficient. This is of interest, as the computation of the confidences is, in comparison to the sensitivities, of great computational effort. Both methods show sufficient levels of confidence, in all sample sizes, to derive qualitative statements.

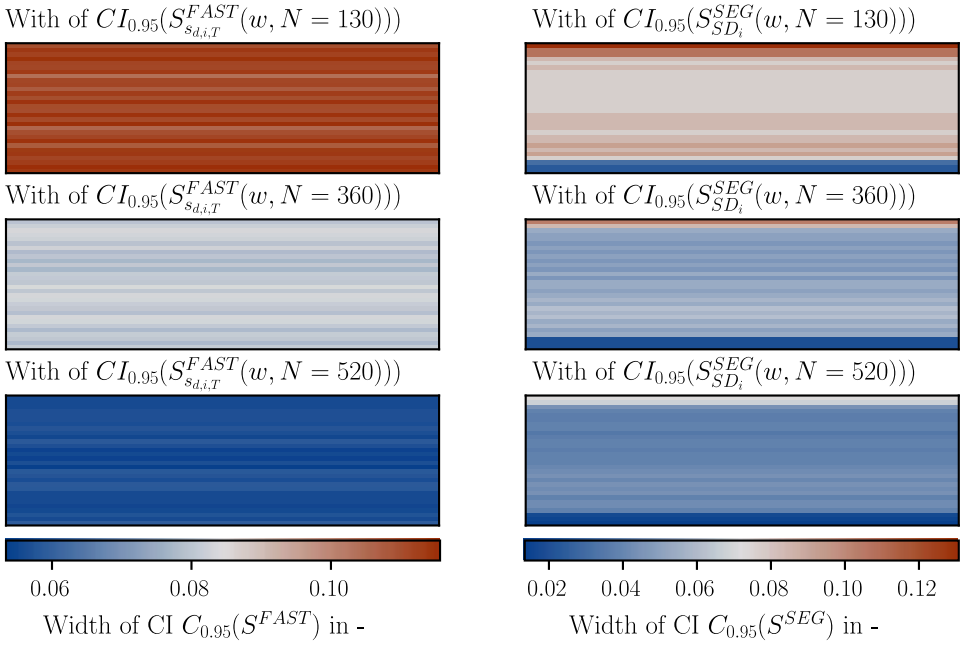

Fig. 4.12: Width of the 95% confidence interval of the Sensitivity Indices computed using the extended FAST method (left) and the segmentation based method (right), for the sample sizes $N = 130, 260, 520$, on a winter day in the last simulation year ($t = 39840\,h$).

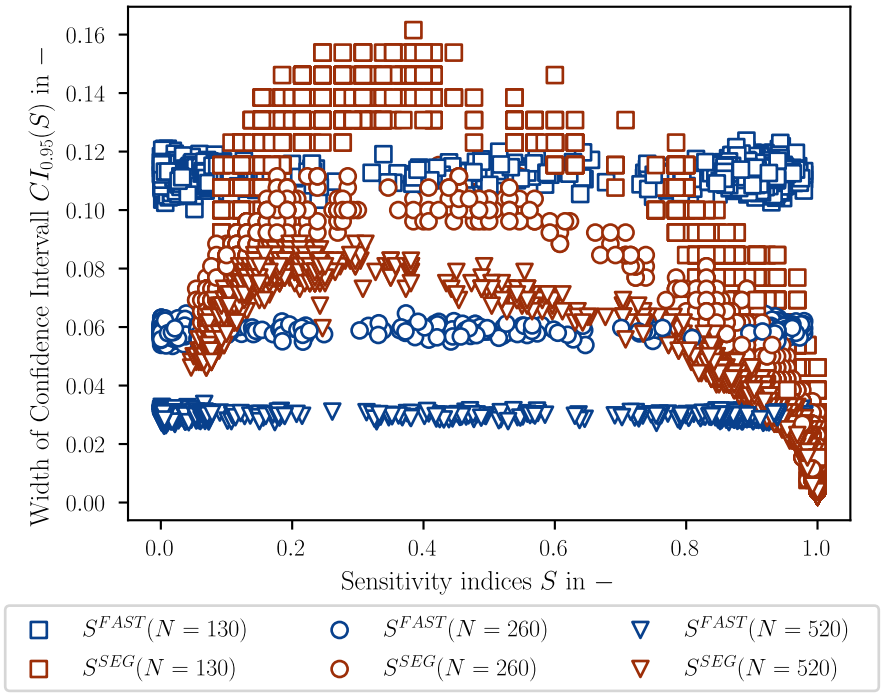

Fig. 4.13: Width of the 95% confidence interval of the Sensitivity Indices over the Sensitivity Indices computed using the extended FAST method (blue) and the segmentation based method (red), for the sample sizes $N = 130, 260, 520$, in any cells at any time t.

Investigation of the convergence behaviour of the SA methods through comparision of the Sensitivity Indices for higher and lower sample sizes, suggest similar results, Fig. 4.14. The eFAST method shows better performance for lower sample sizes, with more consistent spreading. The segmentation based method shows clustering of the sensitivities, higher spreading, and generally less data points around $S = 0.5$.

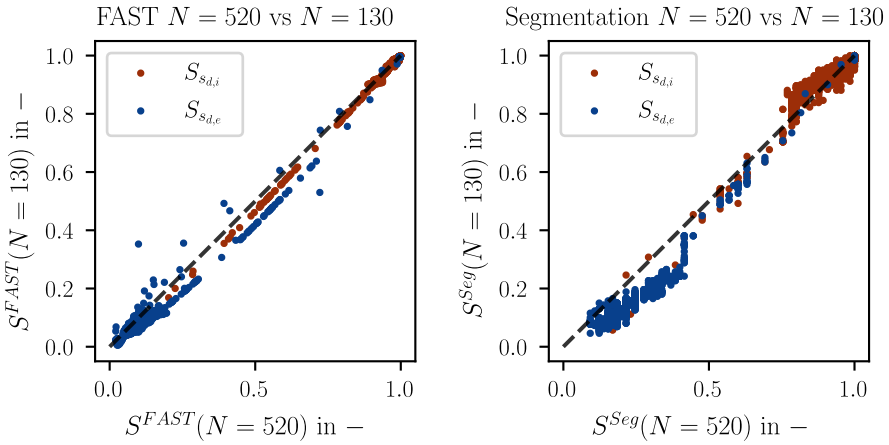

Fig. 4.14: Convergance behaviour of the used SA methods through compasrision of Sesitivity Indices for lower (N=130) and higher (N=520) sample sizes, with separation of the uncertain variables.

Comparison of the methods by the Sensitivity Indices in any point at any time, shows that the segmentation based method overestimates mid to low sensitives and underestimates mid to high sensitivities. Visual evaluation suggests no correlation of this behaviour with the sample size.

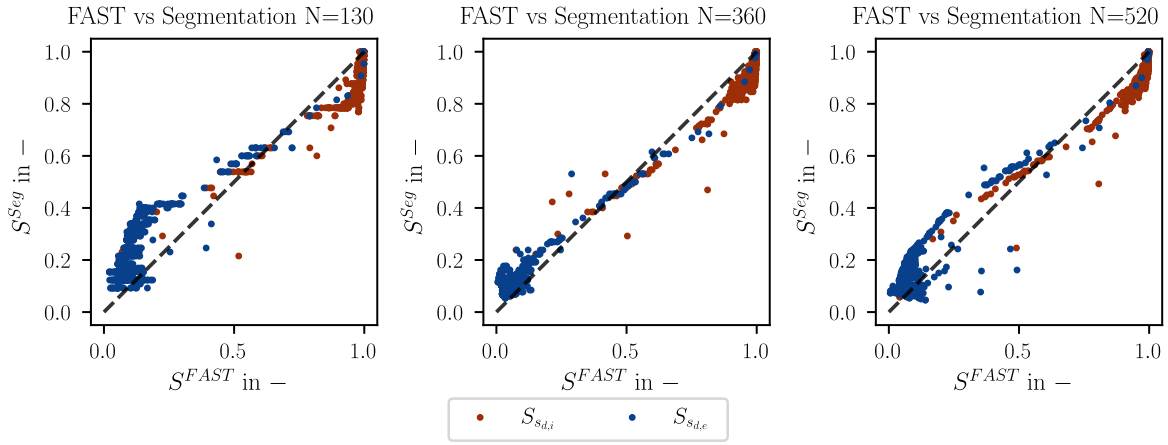

Fig. 4.15: Comparison of the Sensitivity Indices computed using the extended FAST method and the segmentation based method, for the sample sizes $N = 130, 260, 520$, in any cells at any time t.

Up to this point all samples used for the segmentation based method have been generated using the LHC method. As discussed in Sec. 2.2.3.1, the search curve sampling should generate uniformly

distributed samples in the K-space. This should allow the application of the segmentation based methods, with expectation of comparable results to using the LHC sampling method. The results in Fig. 4.16 are consistent with this assumption, showing the majority of data points inside the 95% confidence intervals computed using the initial LHC sample.

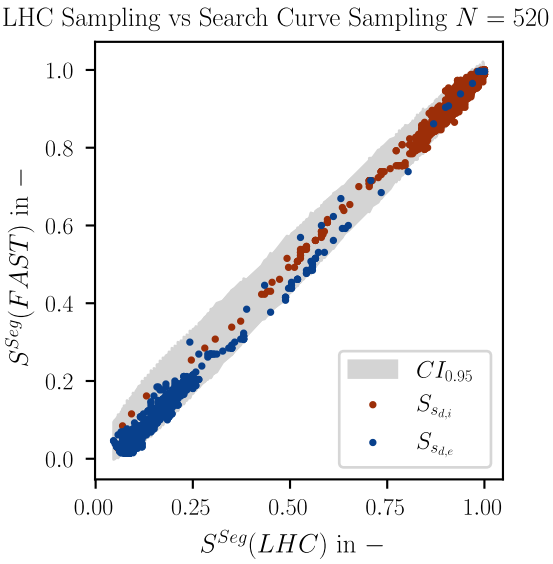

Fig. 4.16: Comparison of the Sensitivity Indices computed using the segmentation based method, on both LHC and search curve sampling, in any cells at any time t.

With this established, the in Sec. 4.3 computed Sensitivity Indices using the segmentation based method, are based on search curve sampled data.

4.3 Application of Sensitivity Analysis in the hygrothermal analysis process

To test the capabilities for the utilization of SA in hygrothermal analysis the complexity of the construction is risen, by consideration of convective heat and moisture transport. Fig. 4.17 shows the model of a flat roof construction, consisting of oak boarding with a spruce beam and blow-in cellulose insulation in between. On the outside roof sealing and on the inside a vapour-variable vapour barrier are applied. The construction is subject to realistic climate conditions. The used boundary conditions, as well as the used material data can be found in Sec. A.1.3.

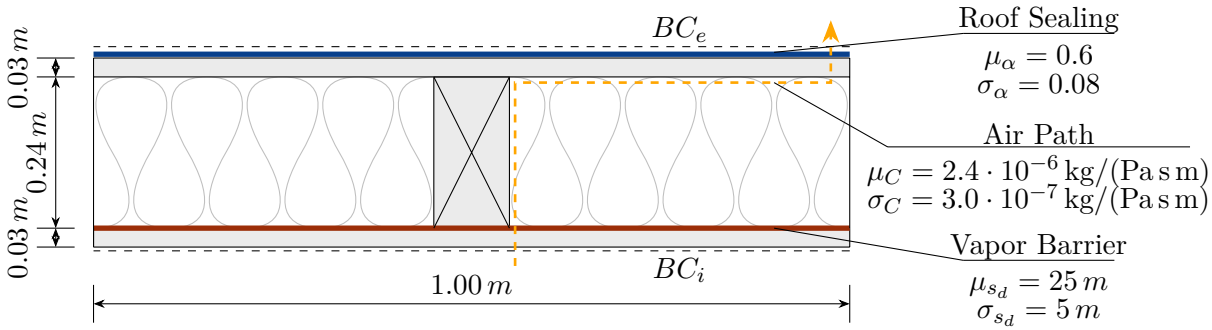

Fig. 4.17: Set up of the two-dimensional flat roof problem consisting of three uncertain input parameters, the s_d-value of the interior vapour barrier s_d, the absorptivity of the exterior roof sealing α, and the air flow coefficient of the gap induce air path C. The domain has two adiabatic boundaries and boundary conditions resembling realistic indoor BC_i and outdoor BC_e climate.

The hygrothermal performance of a building component can be evaluated based on different criteria. ("ÖNORM B 8110-2:2020-01," 2020) lists what criteria have to be fulfilled for buildings in Austria. In this work we want test SA on the basis of two of these criteria. Firstly, the homogenized total moisture content is inspected, to ensure there is no moisture accumulation in the construction. Secondly, the risk of mould growth is investigated, based on the maximum Mould Index in any cell (Ojanen et al., 2011). The failure criterion is defined as $MI \geq 2$, for surfaces in the construction.

Three parameters are identified, as showing both relevant impact and significant uncertainty. The vapour-variable vapour barrier is used to reduce the moisture load, while allowing the construction to dry out to the inside. The uncertainty of the s_d-value is measured by the manufacturer and can be found in product data sheets. In this case the vapour-variability is modelled piecewise linear and the uncertainty is applied for low humidities as shown in Fig. 4.18.

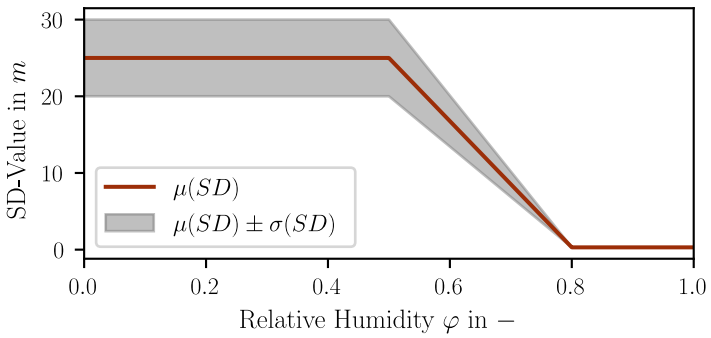

Fig. 4.18: Model function of the vapour variable s_d-value of the vapour barrier over the relative humidity and its uncertainty in lower relative humidities.

To ensure the fault tolerance of the construction an air path through gaps and joints is modelled, with an air flow coefficient of $\mu(C) = 2.4 \cdot 10^{-6} \pm 3.0 \cdot 10^{-7}$ (kg/(s Pa^b)). The mean is chosen in accordance with an air tightness class 3 defined in ("ÖNORM B 8110-2:2020-01," 2020). As a

third uncertainty, the absorptivity of the roof sealing is chosen. Without detailed information provided by manufacturer, the absorptivity has to be assumed, based on the colour of the roof sealing. This holds potential for significant uncertainty due to the subjective colour perception, surface condition and change of absorptivity due to weather exposure. In this case, the sealing is assumed to be grey which according to (Wissenschaftlich-Technische Arbeitsgemeinschaft für Bauwerkserhaltung und Denkmalpflege, 2016) can be assigned to a range of $0.5 \leq \alpha \leq 0.7$ and is therefore chosen as $\alpha = 0.6 \pm 0.08$.

The domain is discretized in two dimensions using the mesh shown in Fig. 4.19. As a sample size $N = 195$ is chosen, the SA is performed using both the eFAST method and the segmentation based method, with an interference factor $M = 4$, and the frequencies $\omega = \{8, 1, 1\}$. For the analysis a duration of ten years is simulated.

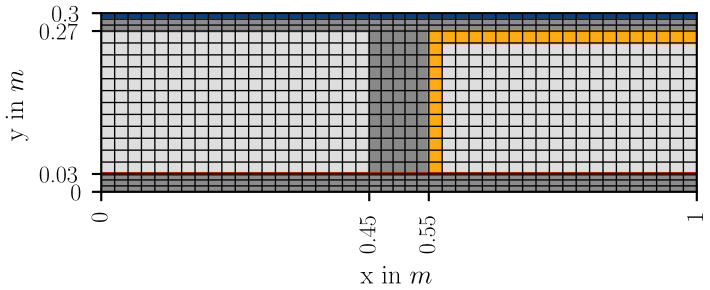

Fig. 4.19: Finite-Volume mesh of the two-dimensional flat roof problem and the position of the uncertain characteristics vapour barrier (red) the roof sealing (blue) and the air path (yellow).

To evaluate the resilience of the construction, two criteria are investigated. Firstly, the homogenized moisture content in the construction (Fig. 4.20) shows accumulation of moisture, after the dry out of the initial moisture. The total moisture content shows significant variation, indicating the relevance of the chosen uncertainties.

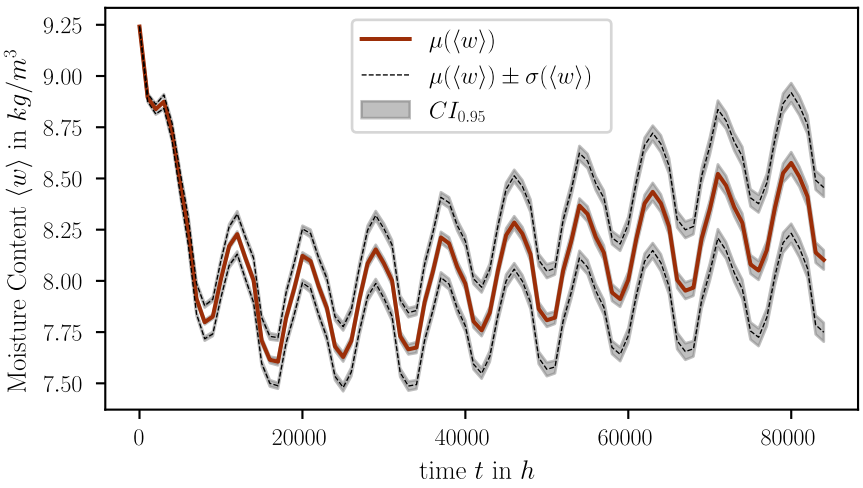

Fig. 4.20: Estimated mean $\mu(\langle w \rangle)$ and standard deviation $\sigma(\langle w \rangle)$ of the homogenized moisture content in the flat roof construction with their respective 95% confidence intervals, evaluated for a sample size $N = 195$, showing significant variation in the homogenized moisture content and indicating moisture accumulation in the construction.

As a second criterion the risk of mould growth is investigated. This is achieved using the Mould Index according to (Ojanen et al., 2011) with a failure criterion of $M \geq 2$ for surfaces inside constructions. As depicted in Fig. 4.21, the construction indicates high probability of failure due to mould growth.

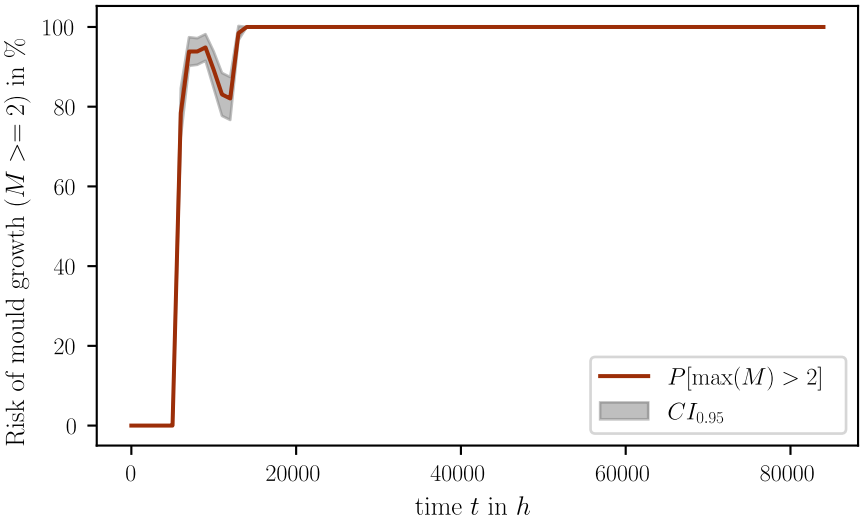

Fig. 4.21: Estimated probability and 95% confidence intervals of failure due to mould growth in the flat roof construction, evaluated for a sample size $N = 195$.

To gain information on how to adapt the construction, the respective Sensitivity indices $S^{FAST}(w)$ and $S^{FAST}(M)$ are inspected. The graphs for the Sensitivity Indices, shown in Fig. 4.22 and Fig. 4.23, indicate that the absorptivity is the dominating factor for both criteria.

The air flow coefficient shows a significant impact on mould growth and the moisture accumulation. Both criteria show no significant sensitivity in respect to the s_d-Value of the vapour barrier for lower relative humidities.

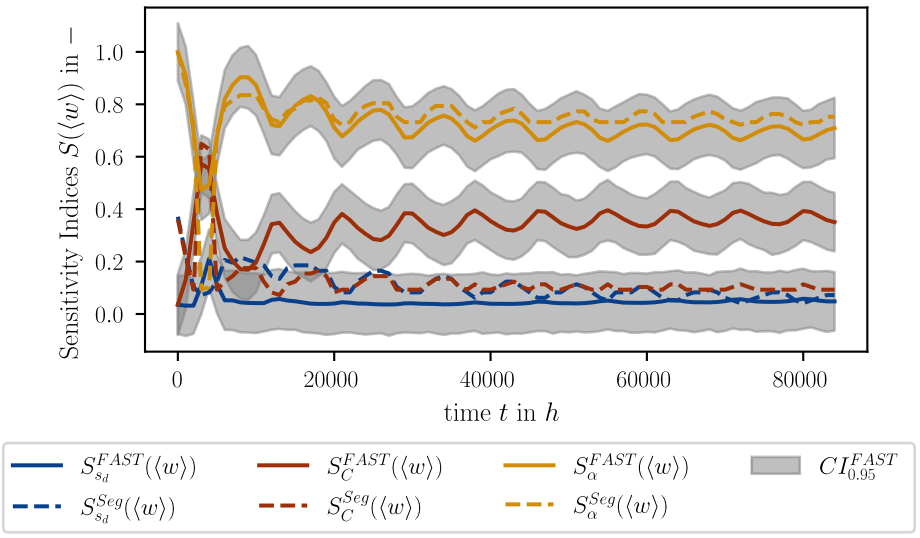

Fig. 4.22: Time dependent behaviour of the Sensitivity Indices $S_{i,T}(\langle w \rangle)$ of the homogenized moisture in a flat roof, in respect to the varying s_d-values of the interior vapour barrier s_d, the absorptivity of the exterior roof sealing α, and the air flow coefficient of the gap induce air path C. Computed using the extended FAST method with sample size $N = 195$.

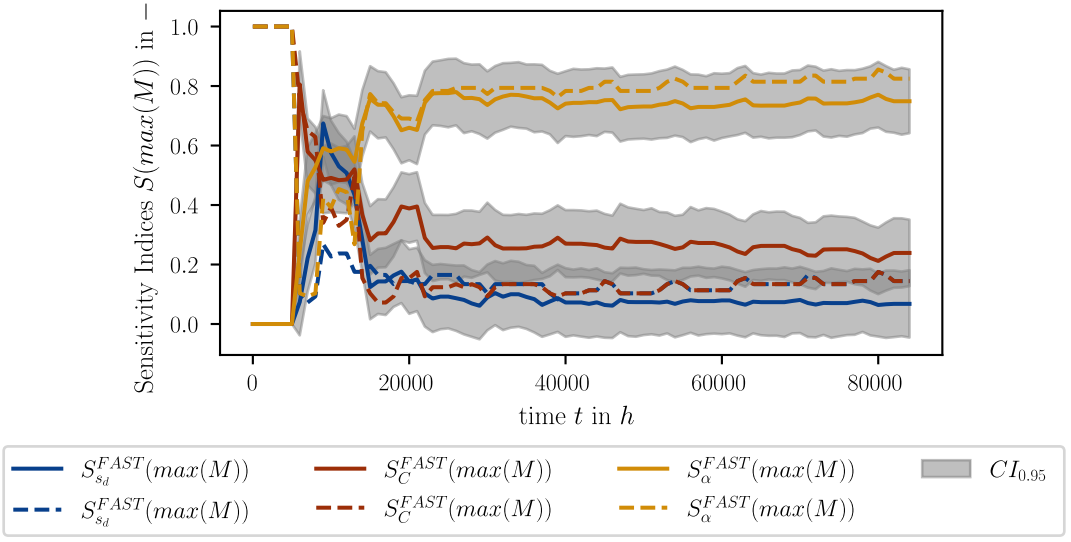

Fig. 4.23: Time dependent behaviour of the Sensitivity Indices $S_{i,T}(max(M))$ of the maximum mould index in the flat roof, in respect to the varying s_d-value of the interior vapour barrier s_d, the absorptivity of the exterior roof sealing α, and the air flow coefficient of the gap induce air path C. Computed using the FAST method with sample size $N = 195$.

The sensitivity indices computed using the segmentation based method $S^{Seg}(w)$ and $S^{Seg}(M)$, estimate similar impact of the absorptivity, but shows significantly lower impact of the air flow coefficient. Plotting the two methods against each other, Fig. 4.24 (left), indicates that they no longer produce consistent results. Increase of sample size used in the segmentation based method (middle) results in better agreement between the methods, suggesting the segmentation based method did not stabilize for the lower sample size. Comparison of the segmentation based method for different sample sizes, with the 95% confidence interval of the lower sample size (right), shows the confidence interval fails to predict the method failure. Further assumptions are drawn from the sensitivities estimated by the FAST method.

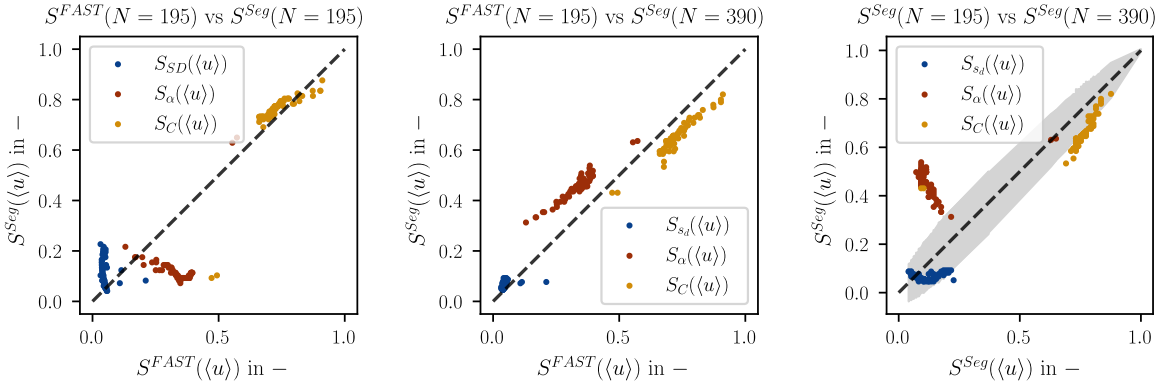

Fig. 4.24: Comparison of the Sensitivity Indices for the homogenized moisture content, computed using the extended FAST method and the segmentation based method, for the sample sizes $N = 195$, at any time t.

With this additional information on the model behaviour the construction is adapted. The absorptivity is adapted to a higher mean value and a reduced standard deviation $\alpha^* = 0.8 \pm 0.03$. An approach to ensure this, could be in situ measurements of the absorptivity and enforcement of periodic cleaning of the sealing. The air flow coefficient is adapted to air tightness class 2, which is resembled by $C^* = 9.6 \cdot 10^{-7} \pm 3.0 \cdot 10^{-7}\,(\mathrm{kg/(s\,Pa^b)})$. This could be enforced trough quality monitoring in prefabrication and in situ review of leakages.

The effect of the adaptions can be seen in Fig. 4.25 and Fig. 4.26. The adapted construction no longer shows indication of moisture accumulation and a significantly reduced risk of failure due to mould growth, suggesting that the through SA as relevant identified input parameter were critical for the performance of the construction.

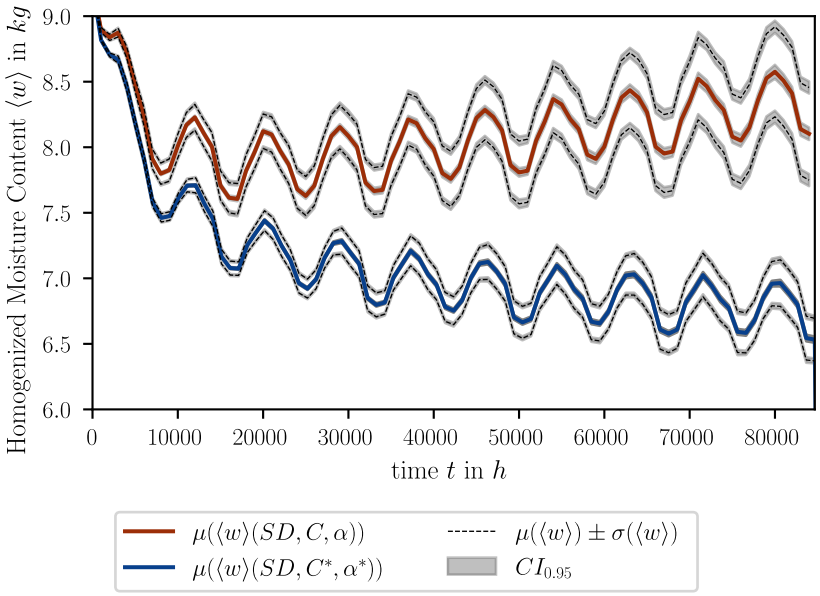

Fig. 4.25: Comparision of the estimated homogenized moisture content before (red) and after (blue) adaptation of the uncertainty of the input variables, for a sample size $N = 195$.

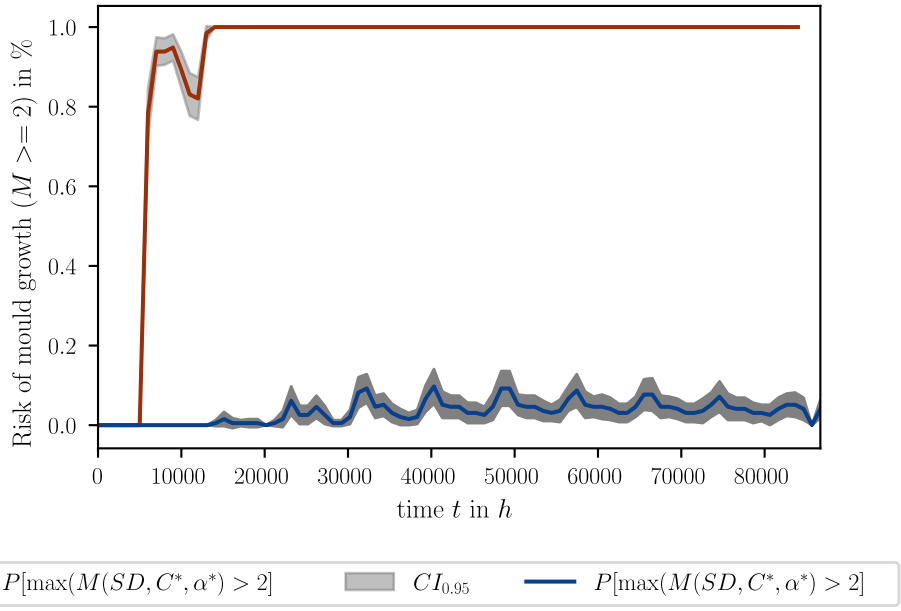

Fig. 4.26: Comparision of the probability of failure due to mould growth before (red) and after (blue) adaptation of the uncertainty of the input variable, for a sample size $N = 195$.

4.4 Discussion

In the heat conduction example, investigated in Sec. 4.1, it is shown that SA provides visually plausible estimations for Sensitivity Indices, which can be used to quantify input output relations. Both methods are able to quantify the relation of local effects in the state variables to the uncertainty of the input parameters. It is notable, that the Sensitivity Indices only represent the ratio of variances and not the variance itself, therefore it is important to inspect the output variance, when drawing conclusions. A result of this behaviour is seen upon investigation of the sensitivity for cases in which the variance of the model output converges to zero. In these case the Sensitivity Indices do not converge to zero, but rather stabilize.

Investigation of reliability of the Sensitivity Indices in Sec. 4.2 brought up significantly different convergence behaviour of the two applied methods. While the FAST method shows confidences independent of the sensitivity, the segmentation based method performs best for high and low sensitivities. The confidence intervals for both methods indicated reliable results, even for lower sample sizes. This is further supported when comparing the results of both methods. Yet, the model output was subject to relatively low variance, which could be the reason for the reliability. Furthermore, the comparison shows patterns of differences in the estimations of the two methods, which seem independent on the sample size. Lastly, it was shown that the segmentation based methods can potentially be applied to samples generated using the search curve method.

Investigation of SA as a tool in the hygrothermal analysis process in Sec. 4.3, showed that SA can be off value for understanding model behaviour and can give qualitative and quantitative guidance in model adaption. Application to low number of variables is of reasonable computational effort. It becomes apparent that the segmentation based method is less robust than the eFAST method, and that the confidence intervals, computed through bootstrapping, are in this case not able to predict the failure of the segmentation based method.

Chapter 5

Conclusion and Outlook

In this work the applicability of SA as a tool in hygrothermal analysis is investigated. To allow this, a probabilistic approach to hygrothermal simulation is performed. After categorization of the models used in hygrothermal simulation, two applicable SA methods are chosen. A simulation framework extending the deterministic model is developed and tested on basis of a case study consisting of three examples with rising complexity. The following conclusions can be drawn from the case study.

SA as a tool in hygrothermal analysis is able to identify the relation of local effects in the state variables to the uncertainty of the input parameters. Furthermore, it is shown, that the Sensitivity Indices hold no information on the scale of the variance and differ in the time dependent behaviour compared to the variance.

The two investigated methods provide qualitative similar results, but they do not necessarily converge to the same Sensitivity Indices. The segmentation based methods shows a lower convergence rate and less robustness for low sample sizes. In the analysed cases, the eFAST method proved to be robust for reasonable sample sizes.

The confidence intervals, computed through bootstrapping, are able to indicate the reliability of the results, once a sensitivity has stabilized, but fail to indicate failure of the segmentation based method for low sample sizes in one case. Further investigation as to why this is the case is needed. Assertion of the reliability of the results remains difficult, therefore it is advisable to use at least two different methods of SA, even when confidence intervals are computed through Bootstrapping.

Lastly, SA proves to be a useful tool to assist in decision-making. It is able to identify why a building component is failing and give quantitative estimation for relevance of parameters. With this information a direct guidance in the adaption of the component, leading to lower probability of failure, is given.

This work provides a starting point for further investigation of SA in hygrothermal simulation on component level. Untouched in this work is the hybrid approach, in which SA is applied in two steps. In the first step a great number of variables is reduced to relevant ones, which are then analysed using more computationally expensive methods. This could prove to be a widely applicable method, with reasonable computational effort and reliable results. Such an approach could be combined with methods like meta-modelling or Gaussian emulators, to further reduce the computational effort.

With probability of failure, in the form of state variables exceeding critical values, being a prominent criterion in hygrothermal analysis, reliability algorithms like FORM and SORM could be of interest. These methods deal with identification of factors driving the failure probability and give approximations for the failure probability. These methods could be possible alternatives to the Monte-Carlo approach.

Acknowledgement

This thesis would not have been possible without the support of my supervisors, Andreas Sarkany and Thomas Bednar. I would like to thank them for their extensive input at all stages of this thesis. I would also like to thank Simon Hinterseer for his commitment in discussing and solving mathematical problems and Bernhard Steiner for his expertise in software development. Finally, I would like to thank Katharina Buczolich for her care, patience, and support during the time of this thesis.

Appendix A

Appendix

A.1 Case Study Input Parameters

A.1.1 Behaviour of Sensitivity Indices using the example of Conductive Heat Transport

This Section includes all parameters used for the computations done in section 4.1.

A.1.1.1 Material Parameters

Tab. A.1: Chosen material parameters of the material A

Kennwert	Symbol	Wert
Thermal Conductivity	λ	$0.2 \pm 0.03\,\mathrm{W/(m\,K)}$
Density	ρ	$100\,\mathrm{kg/m^3}$
Specific Heat Conductivity	c	$1300\,\mathrm{J/(kg\,K)}$

Tab. A.2: Chosen material parameters of the material B

Kennwert	Symbol	Wert
Thermal Conductivity	λ	$0.2 \pm 0.03\,\mathrm{W/(m\,K)}$
Density	ρ	$100\,\mathrm{kg/m^3}$
Specific Heat Conductivity	c	$1300\,\mathrm{J/(kg\,K)}$

Tab. A.3: Chosen material parameters of the material B

Kennwert	Symbol	Wert
Thermal Conductivity	λ	$0.1\,\mathrm{W/(m\,K)}$
Density	ρ	$100\,\mathrm{kg/m^3}$
Specific Heat Conductivity	c	$1300\,\mathrm{J/(kg\,K)}$

A.1.1.2 Confidence Intervals

Confidence intervals computed using $N_R = 400$ resamples for the mean and standard deviation and $N_R = 1000$ resamples for the Sensitivity Indices.

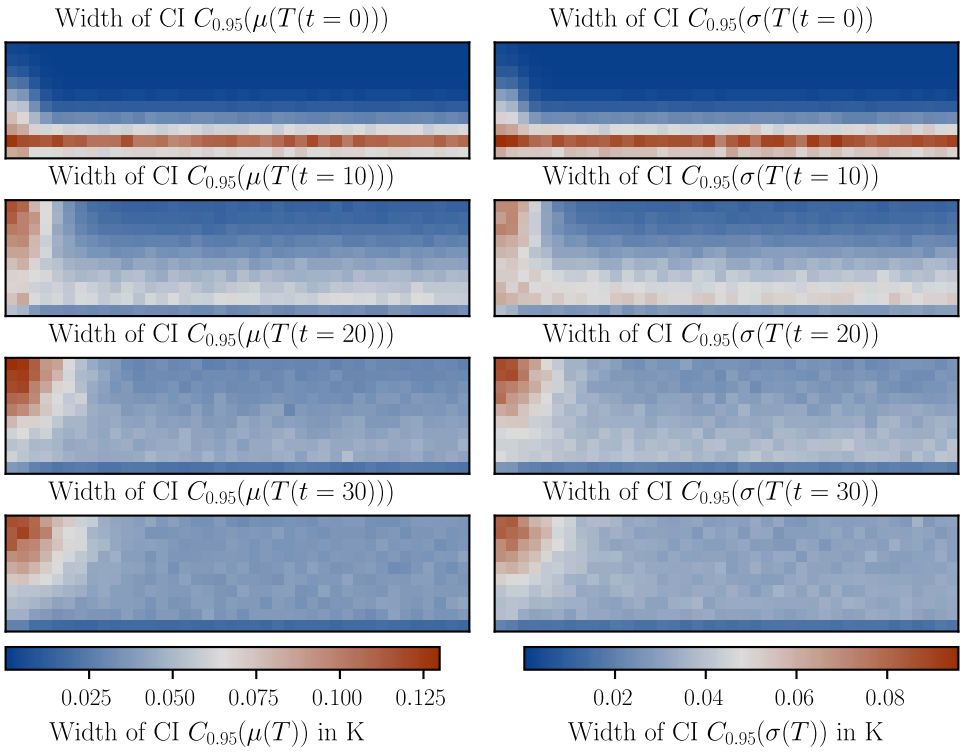

Fig. A.1: Width of the 95% confidence intervall mean $\mu(T)$ and standard deviation $\sigma(T)$ of the Temperature field, at the timesteps $t = 1, 10, 20, 30$ h, showing field dependent sensitivities.

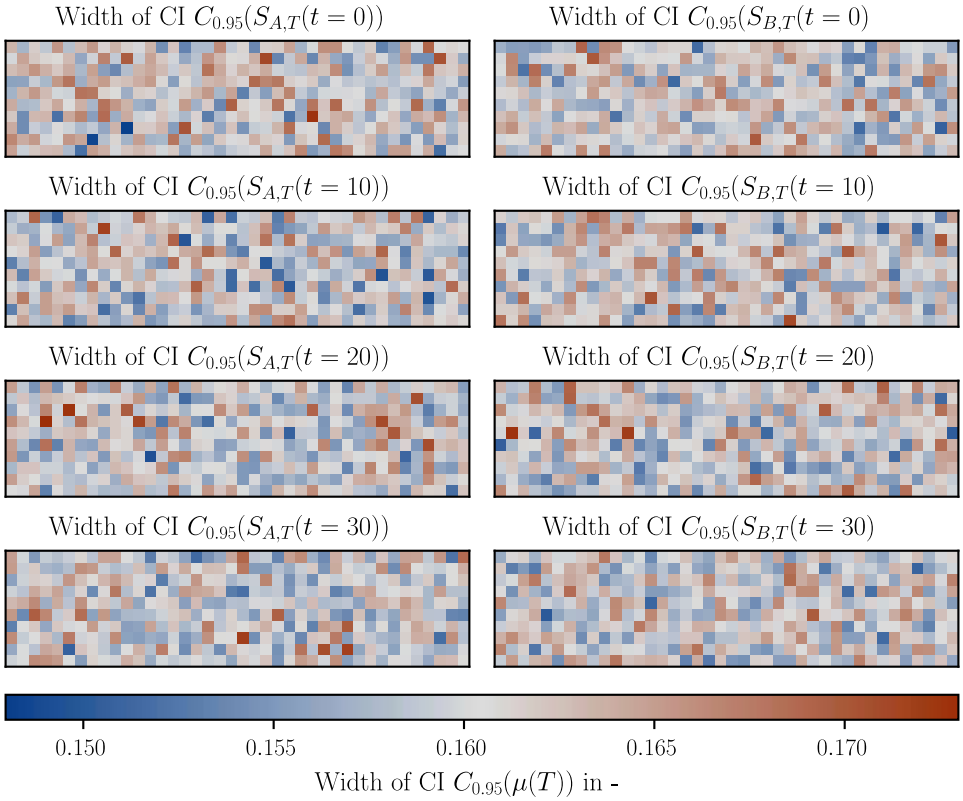

Fig. A.2: Width of the 95% confidence intervall of the Sensitivity Indices computed using the extended FAST method (left) and the segmentation based method (right), of the Temperature field, at the timesteps $t = 1, 10, 20, 30$ h.

A.1.2 Convergence of Sensitivity Indices using the example of diffusive moisture transport in flat roofs

This Section includes all parameters used for the computations done in Sec. 4.2.

A.1.2.1 Material Parameters

Tab. A.4: Chosen material parameters of the blow-in cellulose insulation

Kennwert	Symbol	Wert
Thermal Conductivity dry	$\lambda(\varphi = 0)$	$0.037\,\mathrm{W/(m\,K)}$
Thermal Conductivity moist	$\lambda(\varphi = 1)$	$0.032\,\mathrm{W/(m\,K)}$
Density	ρ	$55.2\,\mathrm{kg/m^3}$
Specific Heat Conductivity	c	$2110\,\mathrm{J/(kg\,K)}$
water vapour resistance factor	μ	3
free water saturation	w_f	$494\,\mathrm{kg/m^3}$
capillary pressure at $w/w_f = 0.5$	s_0	$1.895e4\,\mathrm{Pa}$

Kennwert	Symbol	Wert
fitting parameter	p	0.6

Tab. A.5: Chosen material parameters of the oak boarding

Kennwert	Symbol	Wert
Thermal Conductivity dry	$\lambda(\varphi = 0)$	$0.114\,\mathrm{W/(m\,K)}$
Thermal Conductivity moist	$\lambda(\varphi = 1)$	$0.5695\,\mathrm{W/(m\,K)}$
Density	ρ	$600\,\mathrm{kg/m^3}$
Specific Heat Conductivity	c	$1700\,\mathrm{J/(kg\,K)}$
water vapour resistance factor	$\mu(\varphi = 0)$	150
	$\mu(\varphi = 0.5)$	150
	$\mu(\varphi = 0.8)$	200
	$\mu(\varphi = 1)$	200
free water saturation	w_f	$814\,\mathrm{kg/m^3}$
capillary pressure at $w/w_f = 0.5$	s_0	$3e5\,\mathrm{Pa}$
fitting parameter	p	0.48

Tab. A.6: Chosen material parameters of the roof sealing

Kennwert	Symbol	Wert
SD Value	SD_e	$30 \pm 5\,\mathrm{m}$

Tab. A.7: Chosen material parameters of the vapour barrier

Kennwert	Symbol	Wert
SD Value	SD_i	$30 \pm 5\,\mathrm{m}$

A.1.2.2 Exterior Climate

The exterior climate is based on publicly available weather measurements data from the (Zentralanstalt für Meteorologie und Geodynamik, 2023). For the simulation the following measurement point is used:

Syn. Nr.	Name	Bundesland	Länge	Breite	Stationshöhe	Beginndatum
11361	Bad Ischl	OÖ	13.647223	47.706112	507 m. ü. A.	20070701

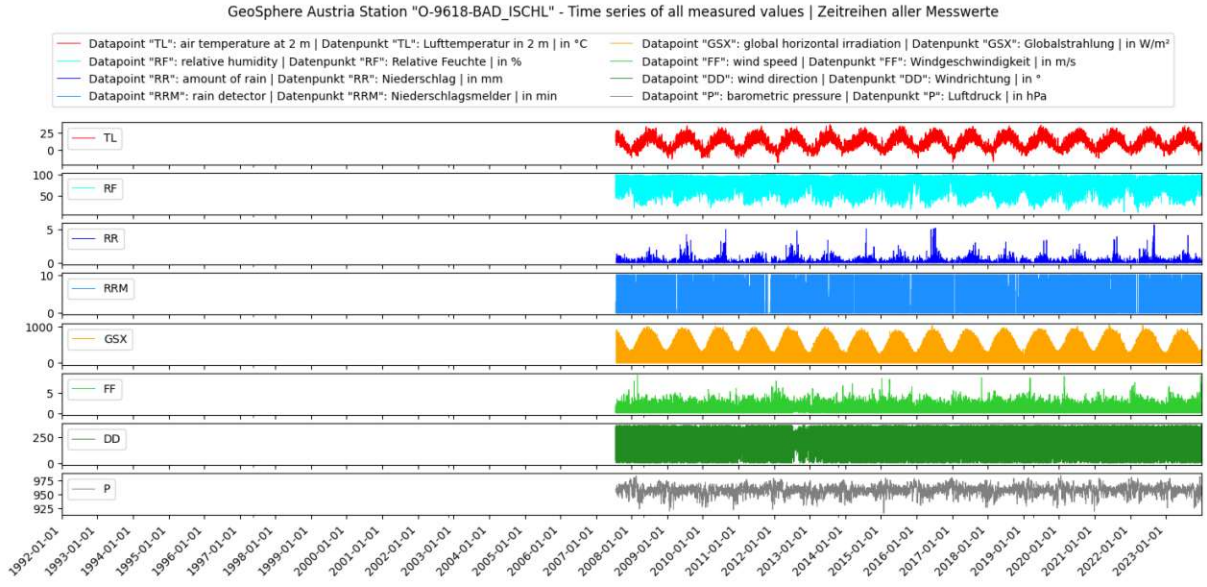

Fig. A.3: Weather data used in the simulation

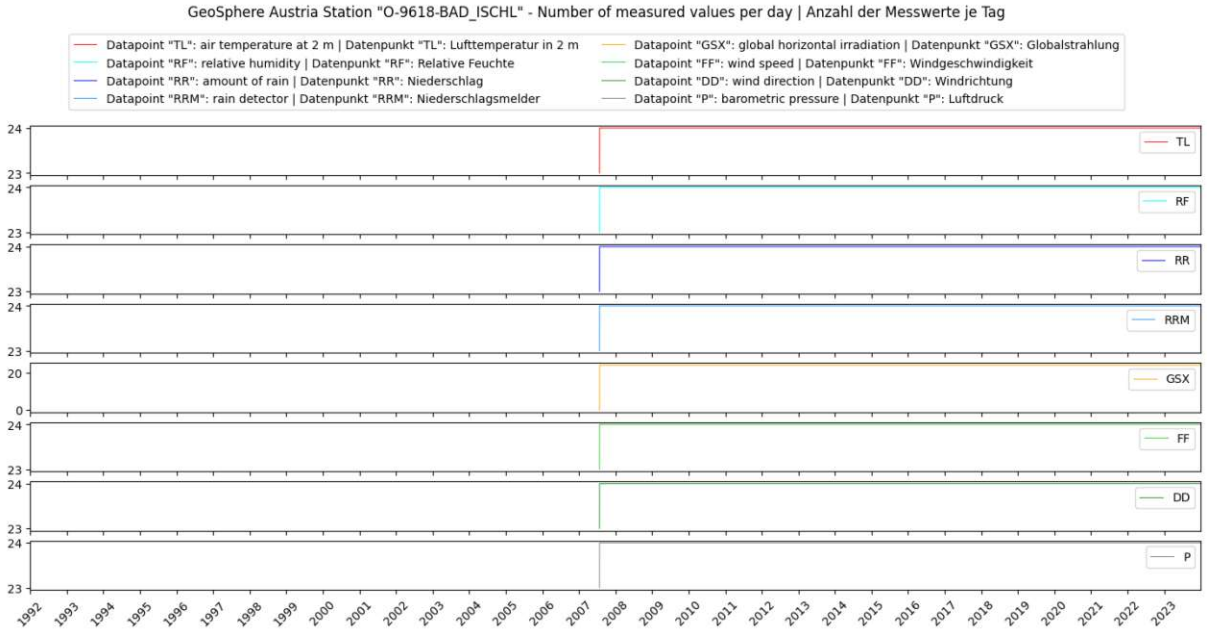

Fig. A.4: Quality of weather data used in the simulation

A.1.2.3 Interior Climate

The interior climate is derived from the exterior climate according to ("ÖNORMB 8110-2 - Wärmeschutz im Hochbau - Teil 2," 2020) as

$$T_i^* = \begin{cases} \text{for } T_{e,m} < 10\,^\circ\text{C} & 22\,^\circ\text{C} \\ \text{for } 10\,^\circ\text{C} \leq T_{e,m} \leq 20\,^\circ\text{C} & 0.5 \cdot T_{e,m} + 17\,^\circ\text{C} \\ \text{for } T_{e,m} > 20\,^\circ\text{C} & 27\,^\circ\text{C} \end{cases}$$

for the interior Temperature and for the moisture excess $\Delta\nu^*$ (kg/m^3) as

$$\Delta\nu^* = \begin{cases} \text{für } T_{e,m} < 0\,°\text{C} & 4\,°\text{C} \\ \text{für } 0\,°\text{C} \leq T_{e,m} \leq 20\,°\text{C} & -0.1625 \cdot T_{e,m} + 4\,°\text{C} \\ \text{für } T_{e,m} > 20\,°\text{C} & 0.75\,°\text{C} \end{cases}$$

The air pressure difference ΔP_s (Pa) is derived from the temperature difference and the height of connected air on the inside z (m) as

$$\Delta P_s = \frac{z}{2} \cdot 3456 \cdot \left(\frac{1}{T_e} - \frac{1}{T_i^*}\right).$$

A.1.2.4 Surface Resistances

Tab. A.9: Interior surface resistances for the flat roof example

Kennwert	Symbol	Wert
thermal resistance	R_{si}	$0.25\,\text{m}^2\,\text{K/W}$
moisture transfer coefficient	β_i	$25 \cdot 10^{-}9\,\text{kg/(m}^2\,\text{s Pa)}$

Tab. A.10: Exterior surface resistances for the flat roof example

Kennwert	Symbol	Wert
thermal resistance	R_{se}	$0.04\,\text{m}^2\,\text{K/W}$
moisture transfer coefficient	β_e	$75 \cdot 10^{-}9\,\text{kg/(m}^2\,\text{s Pa)}$
absorptivity	α	0.12
emissivity	ϵ	0.45

A.1.3 Application of Sensitivity Analysis in the hygrothermal analysis process

This Section includes all parameters used for the computations done in Sec. 4.3.

A.1.3.1 Material Parameters

Tab. A.11: Chosen material parameters of the blow-in cellulose insulation

Kennwert	Symbol	Wert
Thermal Conductivity dry	$\lambda(\varphi = 0)$	$0.037\,\text{W/(m K)}$
Thermal Conductivity moist	$\lambda(\varphi = 1)$	$0.032\,\text{W/(m K)}$
Density	ρ	$55.2\,\text{kg/m}^3$
Specific Heat Conductivity	c	$2110\,\text{J/(kg K)}$

Kennwert	Symbol	Wert
water vapour resistance factor	μ	3
free water saturation	w_f	494 kg/m^3
capillary pressure at $w/w_f = 0.5$	s_0	1.895e4 Pa
fitting parameter	p	0.655

Tab. A.12: Chosen material parameters of the oak boarding

Kennwert	Symbol	Wert
Thermal Conductivity dry	$\lambda(\varphi = 0)$	0.14 W/(m K)
Thermal Conductivity moist	$\lambda(\varphi = 1)$	0.12 W/(m K)
Density	ρ	675 kg/m^3
Specific Heat Conductivity	c	1600 J/(kg K)
water vapour resistance factor	$\mu(\phi = 0)$	200
	$\mu(\phi = 0.5)$	200
	$\mu(\phi = 0.8)$	50
	$\mu(\phi = 1)$	50
free water saturation	w_f	500 kg/m^3
capillary pressure at $w/w_f = 0.5$	s_0	2.98e6 Pa
fitting parameter	p	0.556

Tab. A.13: Chosen material parameters of the spruce beam

Kennwert	Symbol	Wert
Thermal Conductivity dry	$\lambda(\varphi = 0)$	0.09 W/(m K)
Thermal Conductivity moist	$\lambda(\varphi = 1)$	0.426 W/(m K)
Density	ρ	455 kg/m^3
Specific Heat Conductivity	c	1500 J/(kg K)
water vapour resistance factor	$\mu(\phi = 0)$	130
free water saturation	w_f	600 kg/m^3
capillary pressure at $w/w_f = 0.5$	s_0	1.78e6 Pa
fitting parameter	p	0.653

Tab. A.14: Chosen material parameters of the roof sealing

Kennwert	Symbol	Wert
SD Value	SD_e	100 m

Tab. A.15: Chosen material parameters of the vapour barrier

Kennwert	Symbol	Wert
SD Value	$SD_i(\varphi = 0)$	$25 \pm 5\,\mathrm{m}$
	$SD_i(\varphi = 0.5)$	$25 \pm 5\,\mathrm{m}$
	$SD_i(\varphi = 0.8)$	$0.3\,\mathrm{m}$
	$SD_i(\varphi = 1)$	$0.3\,\mathrm{m}$

A.1.3.2 Exterior Climate

The exterior climate is based on publicly available weather measurements data from the (Zentralanstalt für Meteorologie und Geodynamik, 2023). For the simulation the following measurement point is used:

Syn. Nr.	Name	Bundesland	Länge	Breite	Stationshöhe	Beginndatum
11361	Bad Ischl	OÖ	13.647223	47.706112	507 m. ü. A.	20070701

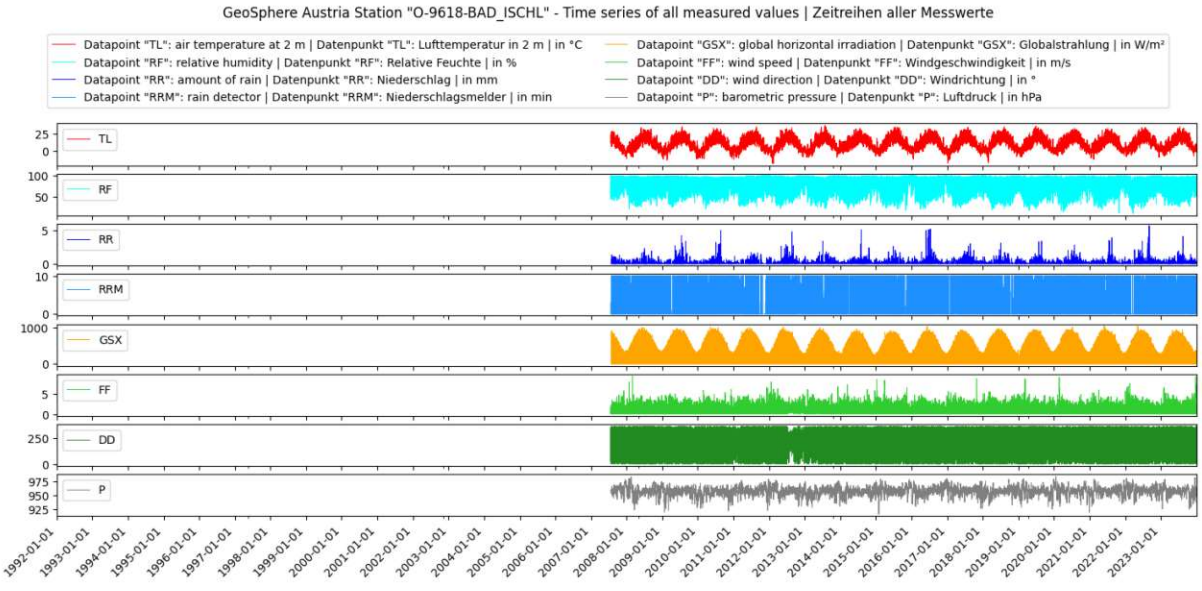

Fig. A.5: Weather data used in the simulation

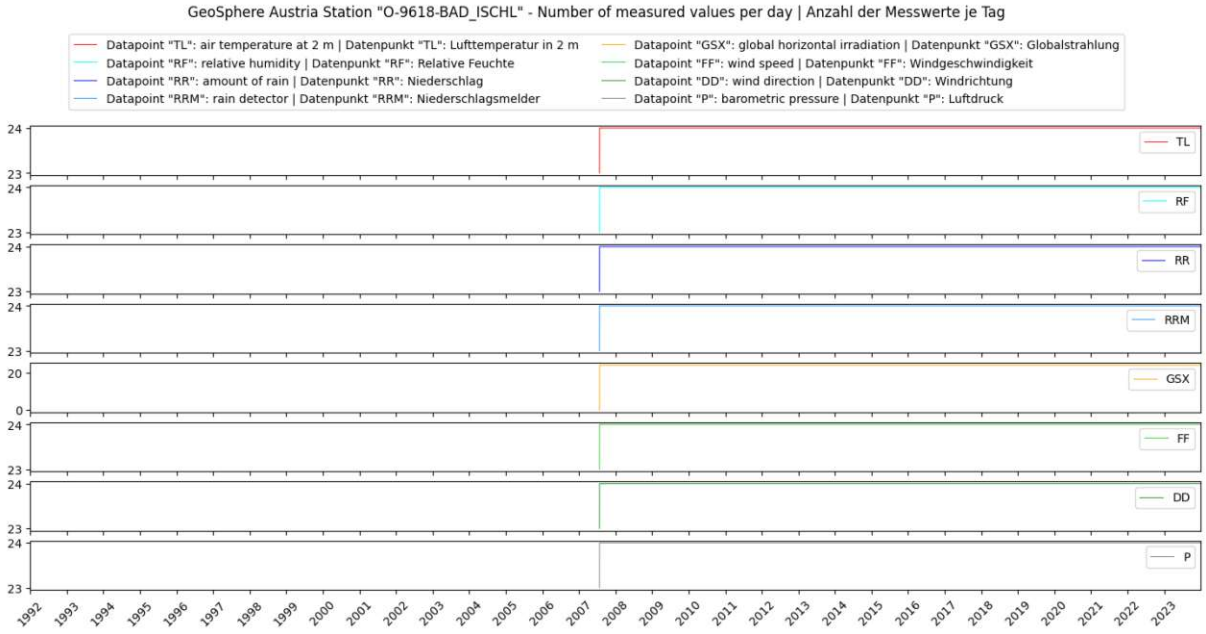

Fig. A.6: Quality of weather data used in the simulation

A.1.3.3 Interior Climate

The interior climate is derived from the exterior climate according to ("ÖNORMB 8110-2 - Wärmeschutz im Hochbau - Teil 2," 2020) as

$$T_i^* = \begin{cases} \text{for } T_{e,m} < 10\,^\circ\text{C} & 22\,^\circ\text{C} \\ \text{for } 10\,^\circ\text{C} \leq T_{e,m} \leq 20\,^\circ\text{C} & 0.5 \cdot T_{e,m} + 17\,^\circ\text{C} \\ \text{for } T_{e,m} > 20\,^\circ\text{C} & 27\,^\circ\text{C} \end{cases}$$

for the interior Temperature and for the moisture excess $\Delta\nu^*\,(\text{kg/m}^3)$ as

$$\Delta\nu^* = \begin{cases} \text{für } T_{e,m} < 0\,^\circ\text{C} & 4\,^\circ\text{C} \\ \text{für } 0\,^\circ\text{C} \leq T_{e,m} \leq 20\,^\circ\text{C} & -0.1625 \cdot T_{e,m} + 4\,^\circ\text{C} \\ \text{für } T_{e,m} > 20\,^\circ\text{C} & 0.75\,^\circ\text{C} \end{cases}$$

The air pressure difference $\Delta P_s\,(\text{Pa})$ is derived from the temperature difference and the height of connected air on the inside $z\,(\text{m})$ as

$$\Delta P_s = \frac{z}{2} \cdot 3456 \cdot \left(\frac{1}{T_e} - \frac{1}{T_i^*}\right).$$

A.1.4 Surface Resistances

Tab. A.17: Interior surface resistances for the two-dimensional flat roof example

Kennwert	Symbol	Wert
thermal resistance	R_{si}	$0.25\,\mathrm{m^2\,K/W}$
moisture transfer coefficient	β_i	$25 \cdot 10^{-}9\,\mathrm{kg/(m^2\,s\,Pa)}$

Tab. A.18: Exterior surface resistances for the two-dimensional flat roof example

Kennwert	Symbol	Wert
thermal resistance	R_{se}	$0.04\,\mathrm{m^2\,K/W}$
moisture transfer coefficient	β_e	$75 \cdot 10^{-}9\,\mathrm{kg/(m^2\,s\,Pa)}$
initial absorptivity	α	0.6 ± 0.08
adapted absorptivity	α^*	0.8 ± 0.03
emissivity	ϵ	0.45

Bibliography

Archer, G.E.B., Saltelli, A., Sobol, I.M., 1997. Sensitivity measures,anova-like Techniques and the use of bootstrap. Journal of Statistical Computation and Simulation 58, 99–120. https://doi.org/10.1080/00949659708811825

Baehr, H.D., 2008. Wärme- und Stoffübertragung. Springer.

Bednar, T., 2000. Beurteilung des feuchte- und wärmetechnischen Verhaltens von Bauteilen und Gebäuden - Weiterentwicklung der Meß- und Rechenverfahren (PhD thesis). Wien, Techn. Univ., Diss.

Bednar, T., Riccabona, C., 2013. Baukonstruktionslehre 4. Verlag Manz.

Camplolongo, F., Saltelli, A., Sørensen, T., Tarantola, S., 2000. Hitchhiker's Guide to Sensitivity Analysis, in: Saltelli, A., Chan, K., Scott, M. (Eds.), Sensitivity Analysis. Wiley.

Chan, K., Tarantola, S., Saltelli, A., Sobol\prime, M.I., 2000. Variance-Based Methods, in: Saltelli, A., Chan, K., Scott, M. (Eds.), Sensitivity Analysis. Wiley.

Conover, W.J., 1980. Practical Nonparametrix Statistics. Wiley.

Cukier, R.I., Fortuin, C.M., Shuler, K.E., Petschek, A.G., Schaibly, J.H., 1973. Study of the sensitivity of coupled reaction systems to uncertainties in rate coefficients. I Theory. Journal of Chemical Physics 59, 3873–3878. https://doi.org/10.1063/1.1680571

Cukier, R.I., Levine, H.B., Shuler, K.E., 1978. Nonlinear sensitivity analysis of multiparameter model systems. Journal of Computational Physics 26, 1–42. https://doi.org/10.1016/0021-9991(78)90097-9

Efron, B., 1992. Bootstrap Methods: Another Look at the Jackknife, in: Kotz, S., Johnson, N.L. (Eds.), Breakthroughs in Statistics: Methodology and Distribution. Springer, New York, NY, pp. 569–593. https://doi.org/10.1007/978-1-4612-4380-9_41

Efron, B., Tibshirani, R.J., 1994. An Introduction to the Bootstrap. Chapman and Hall/CRC, New York. https://doi.org/10.1201/9780429246593

Frigo, M., Johnson, S.G., 2005. The Design and implementation of FFTW3. Proceedings of the IEEE 93, 216–231. https://doi.org/10.1109/JPROC.2004.840301

Hagentoft, C.-E., 2011. Probabilistic Analysis of Hygrothermal Conditions and Mould Growth Potential in Cold Attics. Impact of Weather, Building System and Construction Design Characteristics.

Hagentoft, C.E., 2001. Introduction to Building Physics. Studentlitteratur AB Lund, Sweden.

Hagentoft, C., Janssen, H., Roels, S. et al, 2015. Annex 55, Reliability of Energy Efficient Building Retrofitting - Probability Assessment of Performance and Cost, (RAP-RETRO) - Subtask 2: Probabilistic Tools.

Hens, H., 2017. Building Physics Heat, Air and Moisture.

Herman, J., Usher, W., 2017. SALib: An open-source Python library for Sensitivity Analysis. The Journal of Open Source Software 2, 97. https://doi.org/10.21105/joss.00097

Hinterseer, S., 2024. Parallelization and Performance Analysis of a Hygrothermal Building Component Simulation Using the Example of HAM4D_VIE (PhD thesis). TU Wien.

Hopfe, C.J., Hensen, J.L.M., 2011. Uncertainty analysis in building performance simulation for design support. Energy and Buildings 43, 2798–2805. https://doi.org/10.1016/j.enbuild.2011.06.034

Iooss, B., Da Veiga, S., Janon, A., Pujol, G., 2006. Sensitivity: Global Sensitivity Analysis of Model Outputs and Importance Measures. https://doi.org/10.32614/cran.package.sensitivity

Koda, M., Mcrae, G.J., Seinfeld, J.H., 1979. Automatic sensitivity analysis of kinetic mechanisms. International Journal of Chemical Kinetics 11, 427–444. https://doi.org/10.1002/kin.550110408

McKay, M.D., Beckman, R.J., Conover, W.J., 1979. Comparison of Three Methods for Selecting Values of Input Variables in the Analysis of Output from a Computer Code. Technometrics 21, 239–245. https://doi.org/10.1080/00401706.1979.10489755

Nusser, B., 2012. Flachgeneigte hölzerne Dachkonstruktionen: Systemanalysen und neue Ansätze zur Planung hygrisch robuster flachgeneigter hölzerner Dachkonstruktionen unter Beachtung konvektiver Feuchteeinträge und temporärer Beschattungssituationen. Wien, Techn. Univ., Diss.

Ojanen, T., Peuhkuri, R., Viitanen, H., Lähdesmäki, K., Vinha, J., Salminen, K., 2011. Classification of material sensitivity – New approach for mould growth modeling 2.

ÖNORMB 8110-2 - Wärmeschutz im Hochbau - Teil 2: Wasserdampfdiffusion, -konvektion und Kondensationsschutz, 2020.

Pang, Z., O'Neill, Z., Li, Y., Niu, F., 2020. The role of sensitivity analysis in the building performance analysis: A critical review. Energy and Buildings 209, 109659. https://doi.org/10.1016/j.enbuild.2019.109659

Panico, S., Larcher, M., Marincioni, V., Troi, A., Baglivo, C., Congedo, P.M., 2023. Identifying key parameters through a sensitivity analysis for realistic hygrothermal simulations at wall level supported by monitored data. Building and Environment 229, 109969. https://doi.org/10.1016/j.buildenv.2022.109969

Saltelli, A., Annoni, P., Azzini, I., Campolongo, F., Ratto, M., Tarantola, S., 2010. Variance based sensitivity analysis of model output. Design and estimator for the total sensitivity index. Computer Physics Communications 181, 259–270. https://doi.org/10.1016/j.cpc.2009.09.018

Saltelli, A., Chan, K., Scott, M., 2000. What is Sensitivity Analysis, in: Sensitivity Analysis. Wiley.

Saltelli, A., Tarantola, S., Chan, K.P.-S., 1999. A Quantitative Model-Independent Method for Global Sensitivity Analysis of Model Output. Technometrics 41, 39–56. https://doi.org/10.1080/00401706.1999.10485594

Sarkany, A., 2019. Von der hygrothermischen Bauteilsimulation zur Einschätzung des Risikos eines Feuchteschadens– Implementierung der Berechnung des MouldIndex in HAM4D_VIE. [object Object].

Sarkany, A., Bednar, T., 2021. Hygrothermal simulation and risk evaluation - The impact of discretization on numerical results and performance. Journal of Physics: Conference Series 2069, 012033. https://doi.org/10.1088/1742-6596/2069/1/012033

Schroeder, W.J., Martin, K., Lorensen, W.E., Avila, L.S., Martin, K.W., Lorensen, B., 2006. The visualization toolkit: An object-oriented approach to 3D graphics, 4. ed. ed. Kitware, Inc, Clifton Park, NY.

Sobol, I.M., 2001. Global sensitivity indices for nonlinear mathematical models and their Monte Carlo estimates. Mathematics and Computers in Simulation 55, 271–280. https://doi.org/10.1016/S0378-4754(00)00270-6

Wärmeschutz im Hochbau - Teil 2: Wasserdampfdiffusion,-konvektion und Kondensationsschutz, 2020.

Wegerer, P., Bednar, T., 2017. Hygrothermal performance of wooden beam heads in inside insulated walls considering air flows. Energy Procedia 132, 652–657. https://doi.org/10.1016/j.egypro.2017.09.710

Wissenschaftlich-Technische Arbeitsgemeinschaft für Bauwerkserhaltung und Denkmalpflege, 2016. WTA Merkblatt 6-8:2016-08.

Zentralanstalt für Meteorologie und Geodynamik, 2023. Messdaten Wien Hohe Warte — 1992-2023.

Zhao, J., Plagge, R., Nicolai, A., Grunewald, J., Zhang, J.S., 2011. Stochastic study of hygrothermal performance of a wall assembly—The influence of material properties and boundary coefficients. HVAC&R Research 17, 591–601. https://doi.org/10.1080/10789669.2011.585421

Zhao, J., Plagge, R., Ramos, N.M.M., Lurdes Simões, M., Grunewald, J., 2015. Concept for development of stochastic databases for building performance simulation – A material database pilot project. Building and Environment 84, 189–203. https://doi.org/10.1016/j.buildenv.2014.10.030

Zhao, J., Zhang, J.“Jensen”., Grunewald, J., Feng, S., 2021. A probabilistic-based method to evaluate hygrothermal performance of an internally insulated brick wall. Building Simulation 14, 283–299. https://doi.org/10.1007/s12273-020-0702-6